Construction and Building Materials 440 (2024) 137497

Contents lists available at ScienceDirect

Construction and Building Materials

journal homepage: www.elsevier.com/locate/conbuildmat

# Experimental study on impact behaviour of normal strength mortar at cryogenic temperatures and after freeze-thaw cycles

Kaiyi Chi [a], Jun Li [a], Ruizhe Shao [a,*], Longyang Chen [b], Shenchun Xu [c,*], Chengqing Wu [a,*]

[a] School of Civil and Environmental Engineering, University of Technology Sydney, NSW 2007, Australia
[b] School of Aeronautics, Northwestern Polytechnical University, Xi'an 710072, China
[c] Protective Structures Centre, Guangzhou University, Guangzhou 510006, China

ARTICLE INFO

*Keywords:*
Low/Cryogenic temperature
Cryogenic freeze-thaw cycles
Compressive strength
Split tensile strength
Strain rate effect
Dynamic increase factor

ABSTRACT

Concrete structures employed for the storage of Liquefied Natural Gases (LNG) currently undergo temperature as low as −170 °C. These critical engineering structures may also experience dynamic loads such as impact or explosion during service life. Therefore, it is crucial to explore the mechanical response of concrete at intermediate to high strain rates together with low temperatures or cryogenic freeze-thaw (FT) cycles. This study presents experimental research into the combined effects of low temperatures and strain rate on normal strength mortar, providing a preliminary analysis of the dynamic performance of concrete at low and cryogenic temperatures. A Split Hopkinson Pressure Bar (SHPB) device was used to investigate the characteristics of dynamic compression (at strain rates of 40, 80, 120 and 160 $s^{-1}$) and dynamic split tension (at strain rates of 20, 40, 60 and 80 $s^{-1}$) of Normal Strength Mortar (NSM) at different low temperatures. In addition, the dynamic compression (at strain rates of 80, 130 and 180 $s^{-1}$) after cryogenic FT cycles was also explored. The findings revealed that the failure pattern of NSM samples exposed to coupled low temperature or cryogenic FT cycles and high strain rate loading notably varied from that observed under room temperature condition. Both the dynamic compressive and split tensile strengths of NSM increased with the strain rates at all temperatures. At −160 °C, the dynamic compressive and splitting tensile strengths of NSM specimens were greater than those at room temperature (by 10.94 % and 28.29 %, respectively) and −70 °C (by 3.13 % and 4.12 %, respectively). Cryogenic freeze-thaw cycles evidently impacted the material static and dynamic performance. An empirical model was developed to predict the dynamic increase factors (DIFs) for both dynamic compression and splitting tensile strengths of NSM at low/cryogenic temperatures and after freeze-thaw cycles. Scanning electron microscopy (SEM) technique was performed to study and comprehend the microscopic processes and microstructural changes after FT cycles.

## 1. Introduction

Concrete structures can be exposed to low or cryogenic temperatures in engineering applications such as infrastructure in polar regions and Liquefied Natural Gas (LNG) storage facilities like the All Concrete LNG (ACLNG) storage tank. LNG storage tanks operate at temperatures around −165 °C, subjecting the concrete structures to extremely low temperatures and freeze-thaw (FT) cycles. In addition to routine design loads, engineering structures may face unexpected events such as impacts or explosions due to accidents, gas explosions, or deliberate acts of terrorism during their operational lifespan, which induce high strain rates in the constituent materials. With the increasing demand for infrastructure in cold environments and the growing utilisation of LNG storage facilities [1,2], there is a pressing need to develop concrete materials and structures that withstand extreme low temperatures and dynamic loading conditions. Consequently, a comprehensive evaluation of concrete performances and its failure criteria across a broad spectrum of strain rates (see Fig. 1) is crucial for properly designing structures withstanding dynamic loadings and low temperature condition as along with FT cycles.

A number of researchers have devoted to studying the mechanical characteristics of concrete under low and extremely low temperatures [4–10]. This study aims to support the development of scientifically grounded, economically viable designs for structures, ensuring their

* Corresponding authors.
*E-mail addresses:* Ruizhe.Shao@uts.edu.au (R. Shao), Xushenchun@163.com (S. Xu), Chengqing.Wu@uts.edu.au (C. Wu).

https://doi.org/10.1016/j.conbuildmat.2024.137497
Received 11 June 2024; Received in revised form 10 July 2024; Accepted 16 July 2024
Available online 18 July 2024

reliability and safety under extreme cold conditions. It was frequently observed that the strength of concrete was enhanced at low or extremely low temperatures [9,11]. Lee et al. [12] performed a series of experiments across a temperature range from ambient temperature to −70 °C investigating the compressive and splitting tensile strength, elastic modulus as well as Poisson's ratio of concrete, under both monotonic and cyclic loading conditions. Their findings revealed that as the temperature decreased, the characteristics of aforementioned concrete exhibited an increase as compared to ambient temperature conditions. Specifically, the compressive and splitting tensile strength, elastic modulus, and Poisson's ratio at −70 °C were approximately 2.01, 1.50, 2.07, and 1.47 times greater than at 20 °C. Lin et al. [13] extensively reviewed concrete properties including compressive and splitting tensile strength, elastic modulus etc. under low and cryogenic temperatures. It concluded that concrete properties steadily increased until a critical temperature, after which they stabilised or declined slightly. Compressive strength peaked below −100 °C, while the critical range for tensile strength was between −30 and −70°C. Huo et al. [14] demonstrated that moisture content (MC), aggregate type, water to cement ratio (w/c) etc., influenced concrete properties at low temperatures. Moisture content had the most pronounced impact, with higher levels leading to greater enhancements in performance. Several reasons can explain such improvement. First and foremost, when water freezes inside concrete at lower temperatures, it forms a solid interconnected mesh of ice veins that exerts pressure on the concrete, prestressing it and consequently improving its compressive strength due to the presence of a multiaxial stress state [13]. Furthermore, when water freezes within the tiny pores and capillaries present in the concrete, the ice thoroughly occupies and fills these micro-sized voids throughout the material. This complete filling of the capillary pore spaces by ice helps to distribute stresses more evenly within the concrete matrix at low temperatures. By eliminating these microscopic voids, the formation of localized stress concentrations is mitigated, thereby preventing the initiation and propagation of microcracks within the concrete when exposed to low-temperature conditions. Wiedemann's [15] pore model explained variations in the internal formation of concrete at low temperatures owing to water freezing. Five critical stages were identified with distinct effects on strength, including 20–0 °C, 0 °C to −20 °C, −20 °C to −60 °C, −60 °C to −90 °C and −90 °C to −170 °C: shrinkage, ice formation in larger pores (strength increases), ice in smaller pores (strength slows), ice shrinkage reducing pressure (strength increases), and potential peak strength due to opposing effects at ultra-low temperatures. The model highlighted areas for further research like new testing methods. To gain a deeper insight into the reinforcing effects of low temperatures on concrete, Gong et al. [16,17] utilised micro-scale models to investigate the ice formation within concrete pores and the consequent crack propagation. Through the use of differential scanning calorimetry (DSC) and thermoporometry (TPM) techniques, Jiang et al. [18] discovered that the freezing of water present within the pores of concrete (20 ~ −170 °C), particularly in the temperature range from 0 to −50 °C, played a significant role in enhancing the strength of concrete at cryogenic temperatures. The findings revealed that the formation of ice crystals within both the capillary pores and gel pores contributed to the observed increase in concrete strength when exposed to extremely low temperatures.

In regard with cryogenic FT cycles, a comprehensive review have been done by Van [19] and Lin et al. [13]. Shi et al. [20–22] conducted a comprehensive investigation into the effects of cryogenic FT cycles on the mechanical properties of normal strength concrete (NSC). The studies involved subjecting NSC specimens to various temperature ranges, including 20 to −120 °C, −30 to −120 °C, and 10 to −160 °C, with a controlled cooling rate of 1 °C/min. It was observed that as the number of FT cycles increased, the NSC specimens experienced a notable cumulative degradation. This damage manifested as a remarkable reduction in compressive and tensile strength as well as elastic modulus of NSC. Specifically, the repeated exposure to cryogenic temperatures and subsequent thawing cycles led to a progressive deterioration of the concrete microstructure. When water in the concrete's pores freezes, it expands by approximately 9 % in volume [23]. This expansion induces internal stresses, which cause ice lenses or layers to form within the concrete. The growth of these ice lenses leads to cracks and disrupts the microstructure of concrete [24]. On the other hand, concrete, being a composite material, consists of different constituents with varying coefficients of thermal expansion [25]. During cryogenic cooling, these constituents contract at different rates, resulting in the development of internal stresses and microcracks. Upon thawing, the reverse process of expansion occurs, further exacerbating the cracking and damage. As the FT cycles progress, the cumulative effect of this microstructural damage becomes more pronounced, leading to a substantial reduction in the load-bearing capacity and stiffness of the NSC specimens. The impact on the mechanical properties was more severe as the temperature range and the number of FT cycles increased.

As an important component for concrete, there has been limited research exploring the mechanical behaviour of mortar at cryogenic temperature. Rostásy *et al.* [26] investigated the mechanical properties of mortar at −196 °C and after 1, 2, 4, 6, 8 and 12 no. of cryogenic FT cycles. The results revealed that the compressive as well as splitting tensile strength of water-saturated mortar specimen increased up to approximately 250 % and 170 %, respectively, at −196 °C as compared to room temperature. Furthermore, with increased number of FT cycles (ranging from 20 to −170 °C), the compressive as well as splitting tensile strength of mortar specimens declined (around 50 % and 70 % respectively after 12 FT cycles).

A significant number of researchers have studied the dynamic compression [27–31] and dynamic splitting tension [32–34] at normal temperatures. A number of different experimental techniques have been adopted to explore the dynamic behaviour of mortar, including the Split Hopkinson Pressure Bar (SHPB) test, which evidenced the dynamic compressive and splitting tensile strength of concrete dramatically higher than the quasi-static strength. The research on the mechanical characteristics of mortar under low temperature conditions has predominantly concentrated on static or quasi-static mechanical behaviour. However, analysing mortar response to dynamic loads is crucial for its safe use in harsh environments. The research on the dynamic mechanical properties of mortar at low temperatures is missing, only a few studies have focused on the concrete. Jin et al. [35] developed a 3D

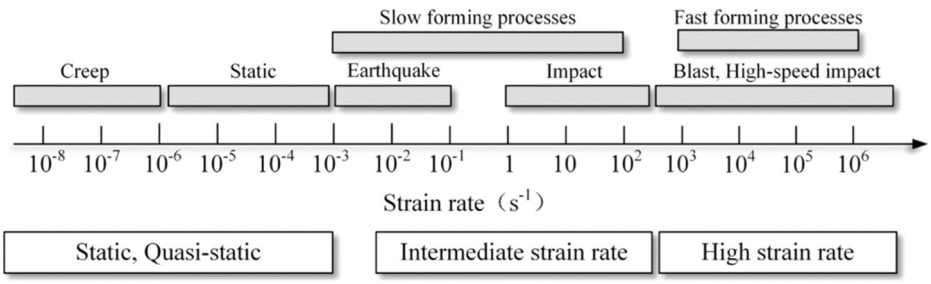


**Fig. 1.** The magnitude of strain rate in different loading scenarios [3].

meso-scale numerical model to investigate the dynamic compressive strength increase factor at strain rate $10^{-5}$–$10^{2}$ $s^{-1}$, with temperature ranging from 20 to −160 °C. Cryogenic temperatures were observed to magnify strain rate sensitivity. Qiao et al. [36] explored the dynamic behaviour of concrete by varying temperature (from 20 °C to −75 °C), strain rate (approximately from 34 $s^{-1}$ to 64 $s^{-1}$), water to cement ratio (w/c) (0.5, 0.6), and maximum aggregate size (12 and 22 mm). It was noted that temperature had the most dramatic impact on dynamic compressive strength, followed by strain rate, w/c as well as the maximum aggregate size. Dynamic compressive strength generally increased with decreasing temperature, reaching a maximum increase ratio of 65 % at −75 °C. Moreover, specific energy absorption (SEA) increased as temperature decreased, indicating improved impact resistance at lower temperatures.

Cryogenic temperatures significantly affect the mechanical properties of concrete, including strength, stiffness and resistance to dynamic loading. Concrete undergoes complex changes in its microstructure under these conditions, which in turn influence its response to dynamic loads such as impacts or blast loadings. Therefore, investigating the dynamic behaviour of normal strength mortar (NSM) under extreme temperature conditions and after cryogenic FT cycles offers valuable insights into its performance and failure mechanisms in real-world engineering applications. This study fills this gap by exploring the dynamic mechanical properties of mortar at 20, −70 and −160 °C temperatures by conducting SHPB tests regarding dynamic compression (40, 80, 120 and 160 $s^{-1}$) and dynamic splitting tension (at strain rates of 20, 40, 60 and 80 $s^{-1}$). In addition, it focuses on the dynamic compressive behaviour of mortar specimens after cryogenic FT cycles varying from 20 to −160 °C in high strain rate (approximately 80, 130 and 180 $s^{-1}$).

## 2. Details of experiment

### 2.1. Materials and specimen preparation

The mix proportion of NSM employed in this experiment is presented in Table 1. The particle size distribution of the sand used in this study is illustrated in Fig. 2 and the sand passed through a 4.75 mm sieve. The physical and chemical properties of cement and coal ash are listed in Table 2. Polycarboxylate ether-based superplasticiser was utilised in mixtures to improve the flowability and workability of mortar. The mixture was poured into the Polyvinyl Chloride (PVC) tube mould with inner diameter of 70 mm. Following initial curing at room temperature (20 ± 2 °C) for 24 hours, the cylindrical specimens were taken out of the PVC tube. After a curing period of 28 days, the specimens were grounded flat on both ends to ensure uniform stress distribution during SHPB testing. The dimensions of the specimen in the dynamic experiment were 70 mm in diameter and 35 mm in height, which is depicted in Fig. 3.

### 2.2. Experimental setup and methodology

#### 2.2.1. Low-temperature test technology

In this experiment, the dynamic compression and splitting tension performance of NSM were investigated at low temperatures of −70 °C and −160 °C. To achieve the desired temperature, the specimens were initially placed inside a low-temperature cooling chamber (depicted in Fig. 4(a)). The inner cooling area of the chamber measured 383 × 228 × 150 mm in length, width and height (as depicted in Fig. 4(b) and (c)), and had the capacity to accommodate 16 specimens simultaneously. Subsequently, the liquid nitrogen Dewar valve was opened, and liquid nitrogen (with a temperature of −196 °C) was gradually introduced into the insulation box, maintaining a cooling rate of 1 °C per minute. The cooling rate could be precisely regulated by a temperature controller, and the temperature change inside the low-temperature chamber was monitored and recorded (refer to Fig. 5). Upon reaching the target temperature, it retained constant for 4 hours to ensure uniform internal and external temperatures of the specimens [37]. Following this, the specimens were expeditiously affixed within the SHPB device to conduct dynamic compressive and splitting tensile experiments.

**Table 1**
Mix composition of NSM (kg/m$^3$).

| Cement | Water | Coal ash | Superplasticizer | Sand |
|---|---|---|---|---|
| 893 | 370 | 70 | 3 | 850 |

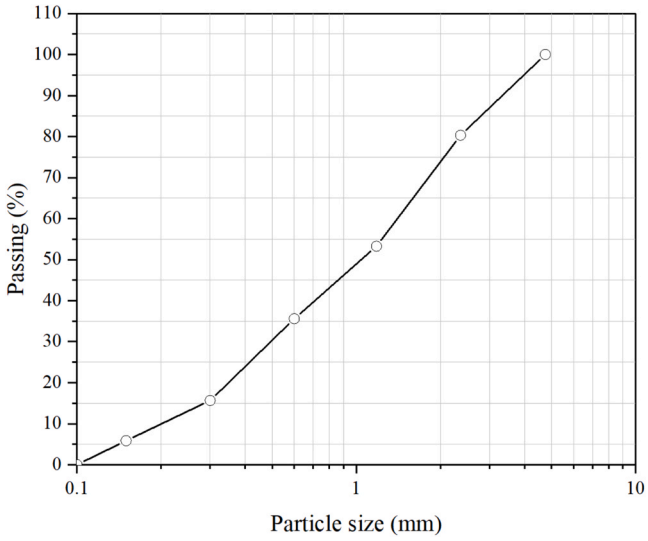


**Fig. 2.** The sieving curve of the sand.

In terms of the cryogenic FT cycles, specimens were placed in the low-temperature chamber with cooling rate 1 °C/min and stayed for 4 hours after reaching the target temperature. Subsequently, the specimens were removed from the chamber and stored indoors at ambient temperature for 24 hours to ensure complete thawing and thermal equilibrium. Herein, one complete FT cycle was defined as the process of cooling the specimen from room temperature down to −160 °C and then allowing it to return to room temperature. The experiment was conducted by varying FT cycles, specifically 2, 4 and 8 cycles, to examine the cumulative effects of repeated cryogenic temperature exposure on the specimens.

#### 2.2.2. Static compressive and splitting tensile test of NSM

The mortar specimens, measuring 70 mm in diameter and 35 mm in height, underwent uniaxial compressive and splitting tensile tests to obtain the basic mechanical properties at 20, −70, and −160 °C. Similarly, the uniaxial compressive strengths of specimens after 2, 4 and 8 no. of cryogenic FT cycles (from 20 to −160 °C) were explored. The experiments were carried out by utilising a 300 ton hydraulic testing machine, with loading applied at a speed of 0.5 mm/min. For the splitting tensile test, the cylindrical specimens were positioned horizontally between the loading surfaces of the compression testing machine. A compressive load was applied along the length of the cylinder at 0.02 mm/min loading rate, diametrically across its width, until the specimen underwent failure by splitting vertically along its diameter.

#### 2.2.3. Dynamic compression and splitting tensile test

The experiment involved different strain rates for compressive and splitting tensile tests: 40, 80, 120, and 160 $s^{-1}$ for compression, and 20, 40, 60, and 80 $s^{-1}$ for splitting tensile test at 20, −70, and −160 °C, as well as dynamic compressive test with strain rate 80, 130 and 180 $s^{-1}$ after 2, 4 and 8 no. of cryogenic FT cycles. Fig. 6 illustrates the setup for dynamic compressive and splitting tensile SHPB tests. The SHPB bar had a diameter of 100 mm and a striker bar length of 500 mm. To enhance the rise time of the incident wave, a pulse shaper was placed between the

**Table 2**
Chemical composition and physical properties of Portland cement and coal ash.

| Materials | Oxide composition % by weight | | | | | | | | Physical properties | |
|---|---|---|---|---|---|---|---|---|---|---|
| | CaO | $SiO_2$ | $Al_2O_3$ | $Fe_2O_3$ | MgO | $SO_3$ | $K_2O$ | $Na_2O$ | Specific gravity ($g/cm^3$) | Avg. particle size (mm) |
| Cement | 63.43 | 18.51 | 5.81 | 3.45 | 2.37 | 3.14 | 0.52 | 0.45 | 3.13 | 0.1 |
| Coal ash | 4.73 | 55.12 | 25.56 | 9.28 | 1.51 | 0.55 | 0.89 | 1.50 | 2.27 | 0.05 |

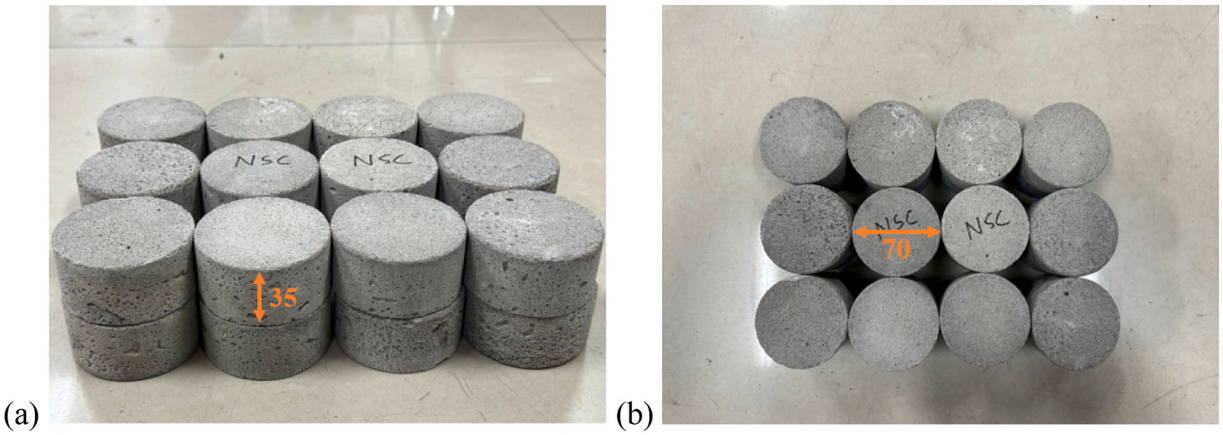


**Fig. 3.** Cylindrical samples after curing (unit: mm).

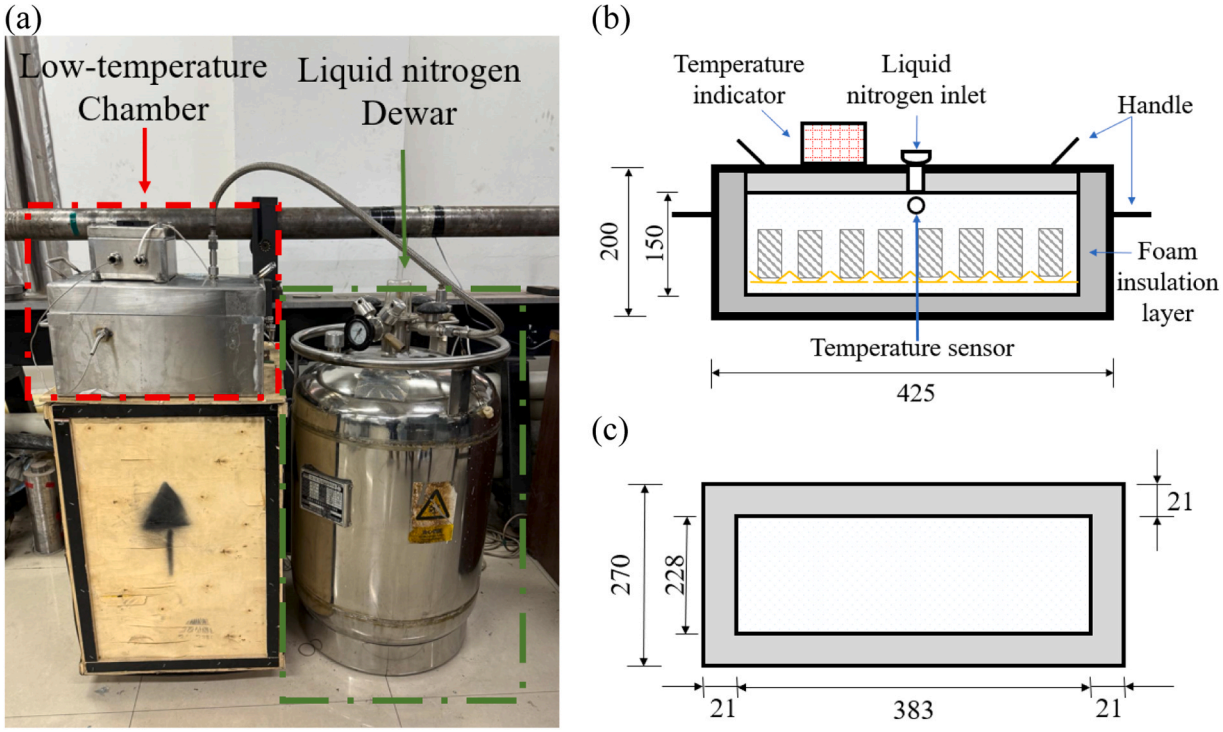


**Fig. 4.** Test setup of NSM at low temperature (a) Cryogenic cooling system (b) Front view of low-temperature chamber (c) Top view of low-temperature chamber (unit: mm).

striker bar and the incident bar as a waveform shaper (refer to Fig. 7) to facilitate the attainment of a uniform stress state within the specimens during dynamic loading, enhancing experimental accuracy and reliability. Strain gauges captured stress wave pulses throughout the testing procedure. Utilising SHPB experimental data, the stress-strain relationship can be derived using the equation [38–40] as below.

$$\sigma = \frac{EA_e}{A_s}(\varepsilon_i + \varepsilon_r + \varepsilon_t) \quad (1)$$

$$\varepsilon(t) = -\frac{2C_0}{L}\int_0^t \varepsilon_r(t)dt \quad (2)$$

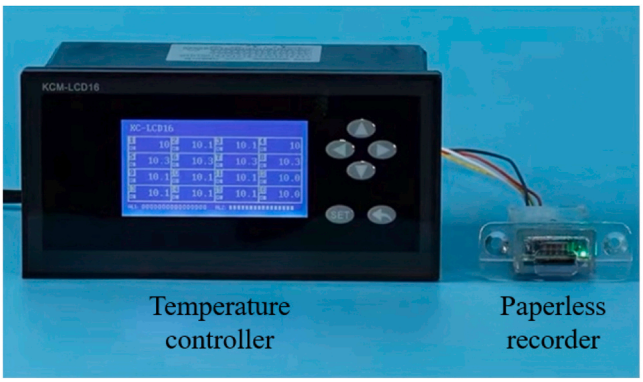


**Fig. 5.** Temperature controlled and paperless recorder.

$$\dot{\varepsilon}(t) = -\frac{2C_0}{L}\varepsilon_r(t) \tag{3}$$

where $\sigma$ is the stress acting at the interface region between the specimen and the loading bar; E denotes the elastic modulus of the incident/transmission bars; $A_e$ and $A_s$ represent the cross-section area of the pressure bar and specimen, respectively. $\varepsilon_i, \varepsilon_r$ and $\varepsilon_t$ are the incident, reflected, and transmitted wave pulses, respectively. $C_0, L$ and $t$ denote the velocity at which the longitudinal wave propagates along the incident/transmission bars, the initial length of the specimen and time, respectively.

Unlike dynamic compressive testing, during dynamic splitting tensile testing, the specimen was placed radially, with the incident bar and the transmitting bar gripping the two sides of the specimen, respectively. Considering that during the splitting test, a line surface contact between the sample and the bar weakened the transmitted wave signal, a semiconductor strain gauge with a higher sensitivity coefficient was installed on the transmitted bar. Simultaneously, a pair of resistance strain gauges were attached to the transmission bar to calibrate the sensitivity coefficient of the semiconductor strain gauges. Based on the one-dimensional stress wave theory, stress, strain and strain rate can be derived for the SHPB splitting tensile test as follows.

$$\sigma = \frac{2P(t)}{\pi DL} = \frac{2EA_e\varepsilon_t(t)}{\pi DL} \tag{4}$$

$$\varepsilon(t) = -\frac{2C_0}{D}\int_0^t \varepsilon_r(t)dt \tag{5}$$

$$\dot{\varepsilon}(t) = -\frac{2C_0}{D}\varepsilon_r(t) \tag{6}$$

where $D$ represents the initial diameter of the specimen and other parameters have mentioned above.

During testing, an ultra-high-speed video camera at frame rates of 5 million frames per second was utilised to capture the behaviour of concrete samples (see Fig. 8). The ultra-high-speed video camera replicated the failure processes for NSM specimens under various temperature and strain rate conditions and provided a wealth of qualitative information. By directly observing the damage progression, crack propagation and fragmentation patterns, it could gain critical insights that complemented the quantitative data from the mechanical tests. This comprehensive visual documentation, paired with the comprehensive mechanical test data, enabled a holistic understanding of the complex interactions between temperature, strain rate and the failure mechanisms of concrete materials.

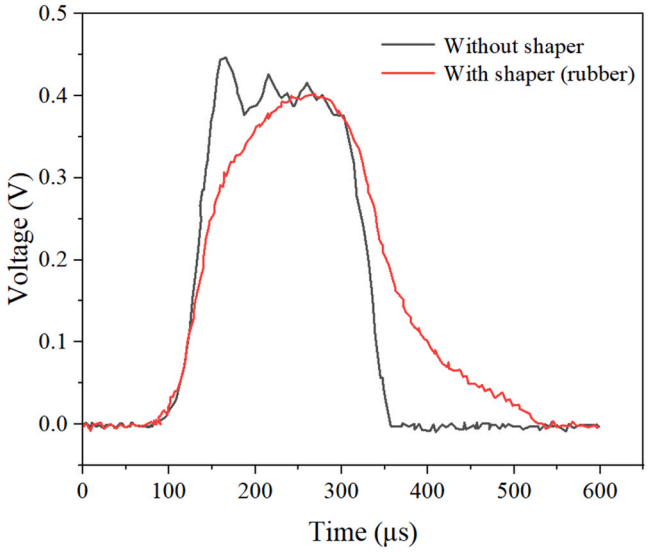


**Fig. 7.** Influence of pulse shaper on incident wave.

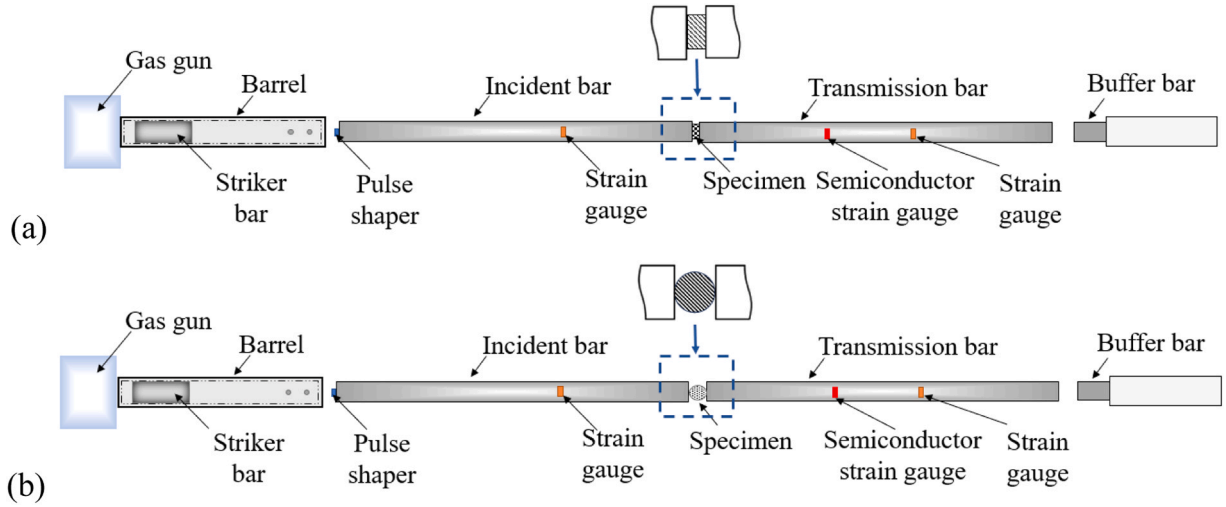


**Fig. 6.** Dynamic testing schematic (a) Compression test (b) Splitting tensile test.

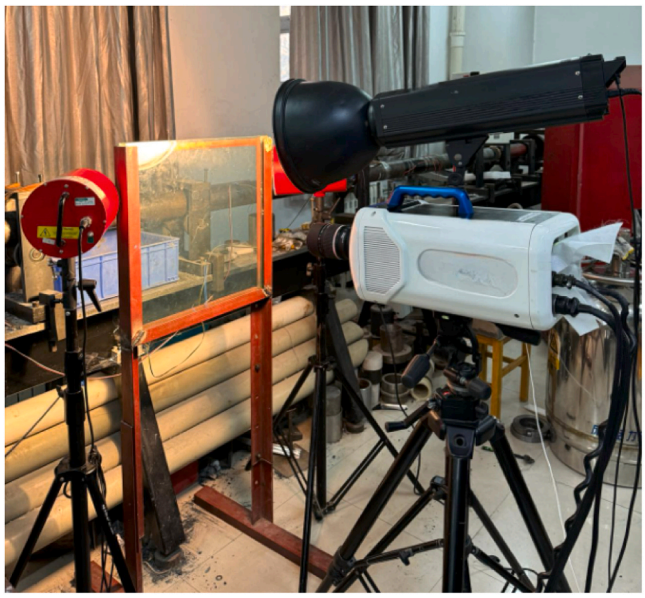

**Fig. 8.** High-speed video camera.

## 3. Experimental results and discussions

### 3.1. Static compressive and tensile behaviour of NSM

The results of uniaxial compressive and splitting tensile strength for NSM at 20, −70, and −160 °C were determined using static tests in Section 2.2.2. The static test results at various temperature are listed in Table 3. When the testing temperature dropped from 20 °C to −70 and −160 °C, the compressive strength was almost linearly increased from 35.26 MPa to 43.19 and 51.76 MPa, with increase of 22.4 % and 46.80 %, respectively. Likewise, as the temperature declined from 20 °C to −70 and −160 °C, the splitting tensile strength rose from 2.52 MPa to 2.81 and 3.10 MPa, respectively, rendering an increase of 11.5 % and 23.02 %. 67, which declined by 5.7 %, 14.6 % and 27.28 % as compared to the room temperature. In terms of static test after cryogenic FT cycles, the uniaxial compressive strength was 33.25, 30.11 and 25.64 MPa after 2, 4 and 8 times FT cycles, which declined by 5.7 %, 14.6 % and 27.28 % as compared to the room temperature (see Table 4). The uniaxial compressive stress-strain curve of NSM under low temperature and after FT cycles is presented in Fig. 9.

### 3.2. Dynamic compressive strength under low temperature

#### 3.2.1. Damage mode of specimens subjected to combined loading

Under combined loading conditions at temperatures of 20, −70 and −160 °C together with strain rates of approximately 40, 80, 120 and 160 $s^{-1}$, remarkable variations in the damage appearance of the specimens were observed, indicating a correlation between temperature and strain rate. Fig. 10 displays the damage forms of NSM at various strain rates under temperatures of 20, −70, and −160 °C, respectively. It was evident that the damage phenomenon of NSM became more pronounced with rising strain rate, and the crushed pieces of damaged concrete gradually decreased in size at the same temperature. The main reason for this phenomenon was that the water freeze forming an ice mesh acted as an internal reinforcement, helping to resist the propagation of cracks and damage through the material. The prestressed state induced by the ice veins can delay or impede the initiation and growth of cracks at lower temperatures. The stiffness of the material increased at lower temperatures, rendering it more resistant to deformation and damage.

**Table 3**
Static test results under low temperature.

| Temperature (°C) | Uniaxial compressive strength (MPa) | Splitting tensile strength (MPa) |
|---|---|---|
| 20 | 35.26 | 2.52 |
| -70 | 43.19 | 2.81 |
| -160 | 51.76 | 3.10 |

**Table 4**
Static test results after cryogenic FT cycles.

| Number of FT cycles | Uniaxial compressive strength (MPa) |
|---|---|
| 2 | 33.25 |
| 4 | 30.11 |
| 8 | 25.64 |

To further elucidate the damage evolution and deformation mechanisms of the specimens under combined loading conditions of varying temperatures (20, −70, and −160 °C) and strain rates (about 40, 80, 120 and 160 $s^{-1}$), detailed images of the testing process were captured using the ultra-high-speed video camera. Fig. 11 displays the dynamic failure of NSM specimens at temperatures of 20, −70 and −160°C, respectively, along with a strain rate of around 80 $s^{-1}$. As compared to the specimens underwent failure at −70 °C, the longitudinal splitting of specimens experienced failure at 20 °C was more severe. It was noteworthy that at −160 °C, the number and depth of cracks were more significant and apparent in comparison with room temperature and −70 °C, as shown in Fig. 11(c). This phenomenon, combined with Fig. 10(c), at which the strain rate was 79.38 $s^{-1}$, suggested that the stiffness of NSM specimens at −160 °C was high, essentially retained the original appearance after the impact, but accompanied by its more brittle characteristics. This observation aligned with the conclusions drawn by Yan and Xie [41] regarding the low-temperature performance of concrete. In general, when the compressive strength of the material rose, the specimen became more brittle. The temperature gradually decreased, the compressive strength of the specimen improved, thus exhibiting brittleness.

In fact, concrete at −160 °C was more brittle than at −70 °C owing to the water freeze in pores. At −160 °C, more water in the concrete pores froze than at −70 °C. The water-to-ice phase transition resulted in a volume expansion of around 9 % as mentioned above, which induced hydraulic pressure and stresses at the ice-pore interfaces [42]. This produced damage and cracks in the concrete microstructure, leading to increased brittleness. In addition, in accordance with Zhang et al. [42], temperatures of −90 °C and lower led to a reduction in the quantity of larger pores and an increase in the quantity of smaller pores. This was because the large pores were collapsed or filled due to the inward deformation caused by the uneven contraction and expansion between different concrete constituents at ultra-low temperatures. The loss of these larger pores rendered the concrete more brittle. Furthermore, Jiang et al. [25] stated that thermal expansion mismatch was also a main reason causing the brittleness at lower temperatures. The thermal expansion coefficients of the concrete components were different from those of ice. As the temperature declined further from −70 to −160 °C, the inconsistent thermal deformations between these materials accumulated, resulting in higher internal stresses and cracking, which increased the brittleness.

#### 3.2.2. Influence of low temperature on the dynamic compressive strength

Fig. 12 illustrates stress-strain curves with different strain rate at 20, −70 °C and −160 °C. It revealed a consistent trend wherein the dynamic compressive strength of concrete exhibited an upward trajectory as the average strain rate increased. Under room temperature conditions, for instance, the dynamic strength of NSM specimens exhibited signal enhancements in contrast with those subjected to lower strain rates. Specifically, when the strain rate escalated from 40 $s^{-1}$ to 80, 120 and 160 $s^{-1}$, the dynamic compressive strength experienced increments of 5.27 %, 18.02 % and 23.91 %, respectively. This trend retained

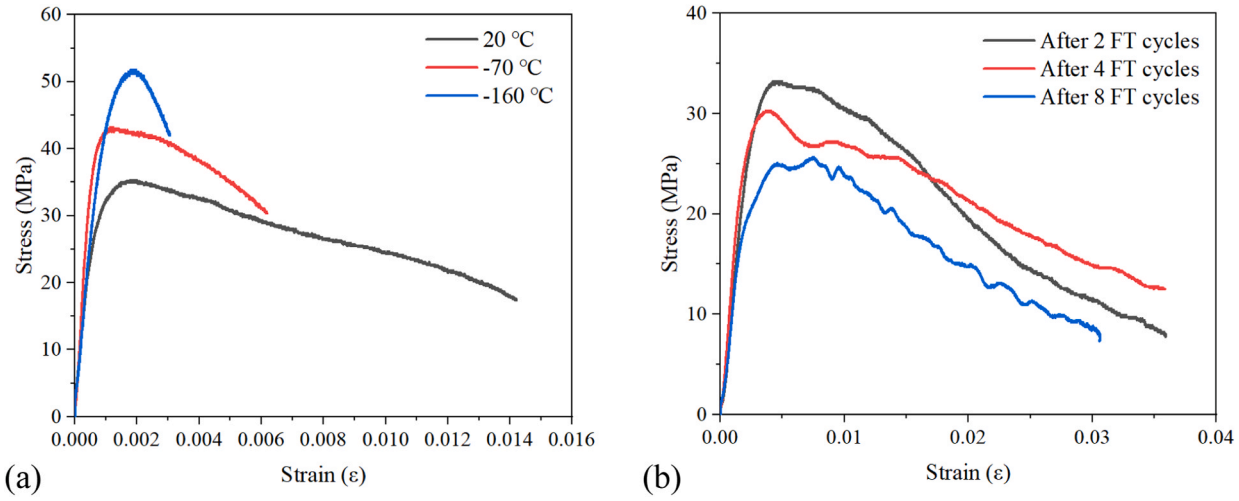


**Fig. 9.** Uniaxial compressive stress-strain curve of NSM. (a) under different low temperatures (b) after various FT cycles.

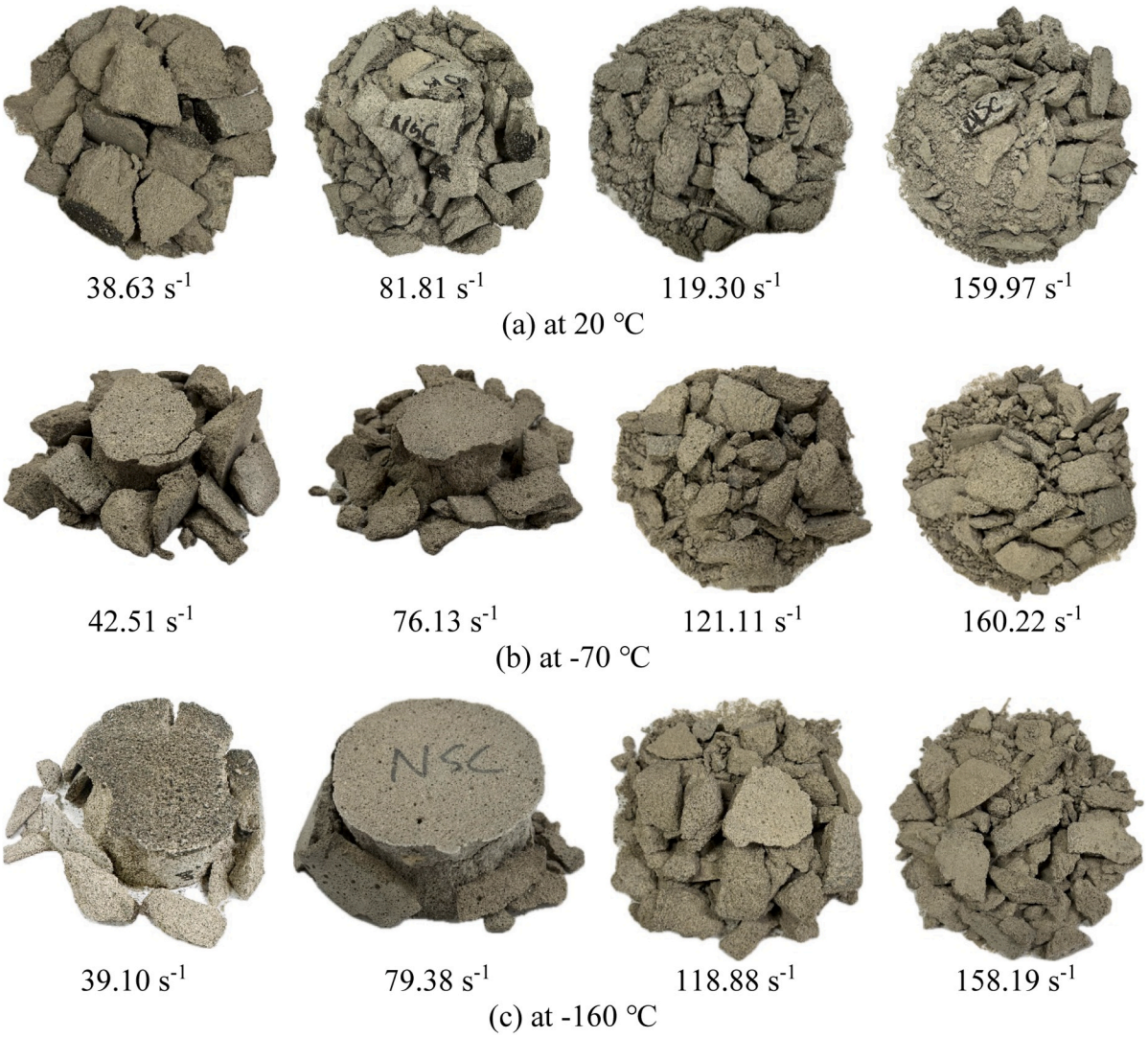


**Fig. 10.** Dynamic compressive failure modes of specimens at different temperatures.

consistent across varying temperatures. In environments as extreme as −70 and −160 °C, the dynamic compressive strength also showcased notable improvements with escalating strain rates. For example, at −70 °C, the strength increased by 10.53 %, 24.33 % and 28.60 % at 80, 120 and 160 $s^{-1}$, respectively, when compared to 40 $s^{-1}$. Similarly, at −160 °C, the strength rose by 4.10 %, 17.22 % and 22.57 % with the same

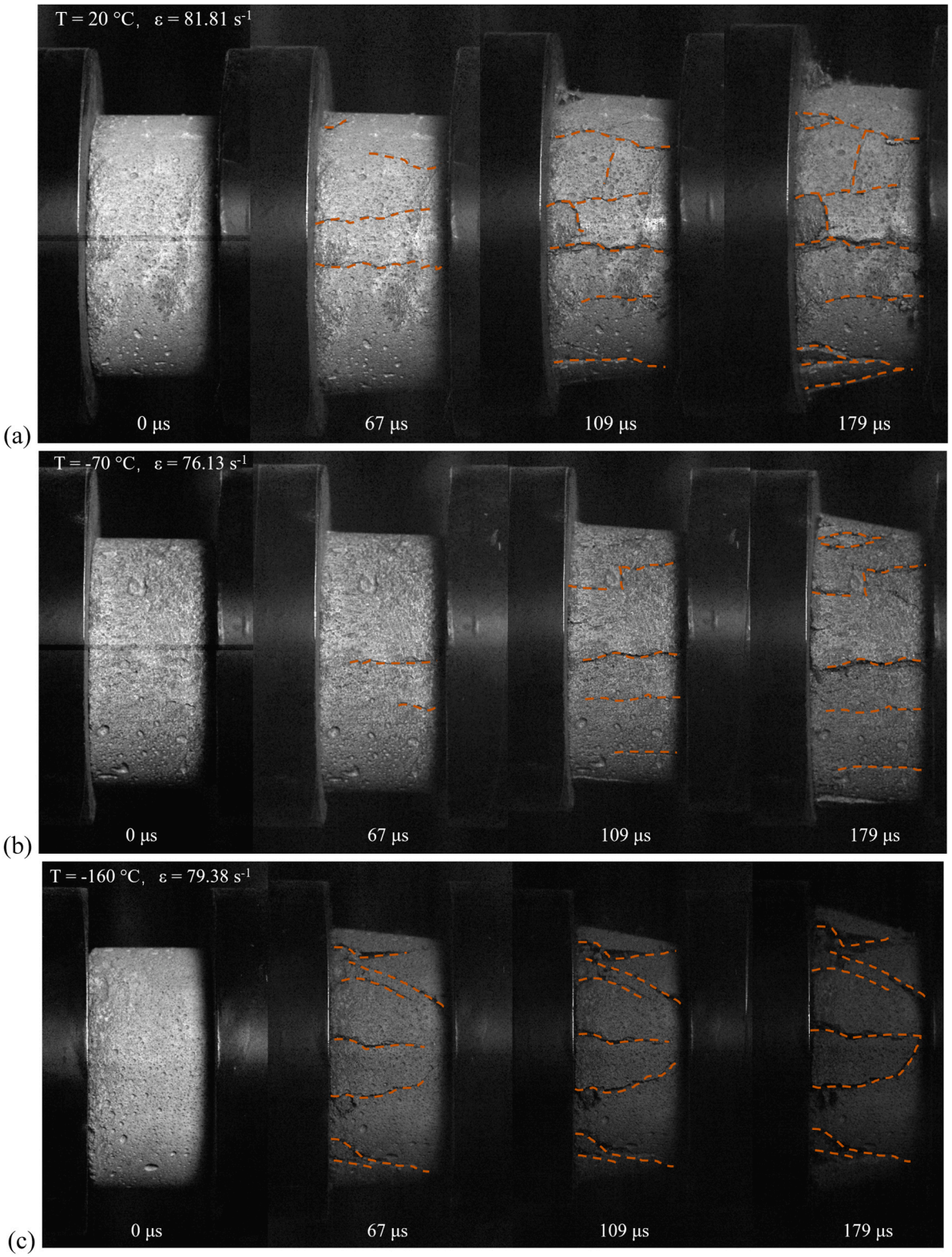


**Fig. 11.** Compression failure process of specimens under different temperature. (a) at room temperature (b) at −70 °C (c) at −160 °C.

increment in strain rates. These data indicated that at the identical temperature, the dynamic strength of concrete dramatically increased with strain rate.

Studying the elastic modulus of NSM under dynamic experiments held significant importance as it constituted a vital mechanical characteristic of concrete materials. Fig. 13 shows a comprehensive overview of the dynamic compressive strength and elastic modulus variations observed in NSM specimens subjected to different temperatures and strain rates. It was evident that, at the same average strain rate, the dynamic compressive strength gradually increased with decreasing temperature. The elastic modulus representing the proportional relationship between stress and strain could be estimated through the slope

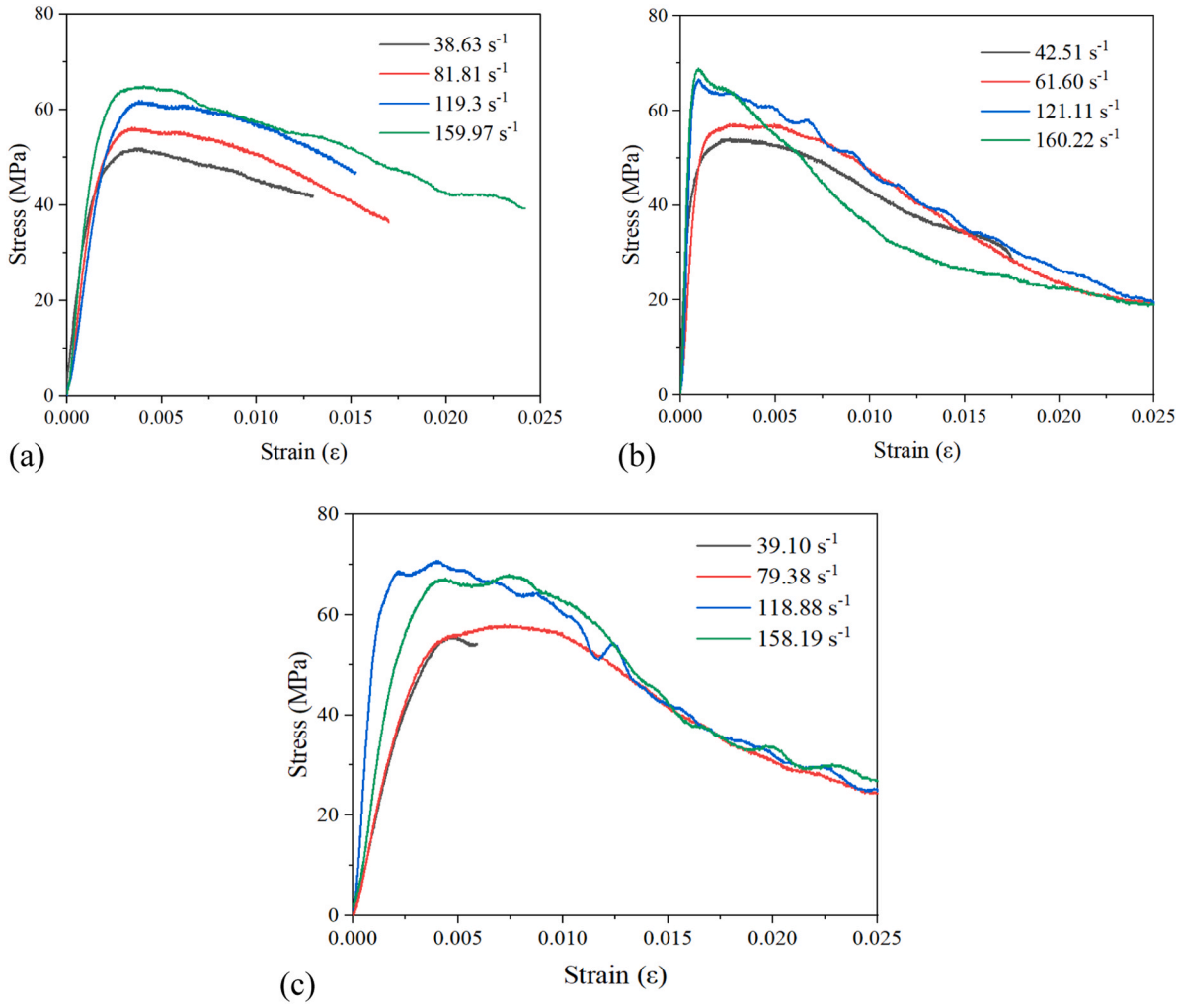


**Fig. 12.** Compression strain-stress curve at different temperatures with various strain rates. (a) at 20 °C (b) at −70 °C (c) at −160 °C.

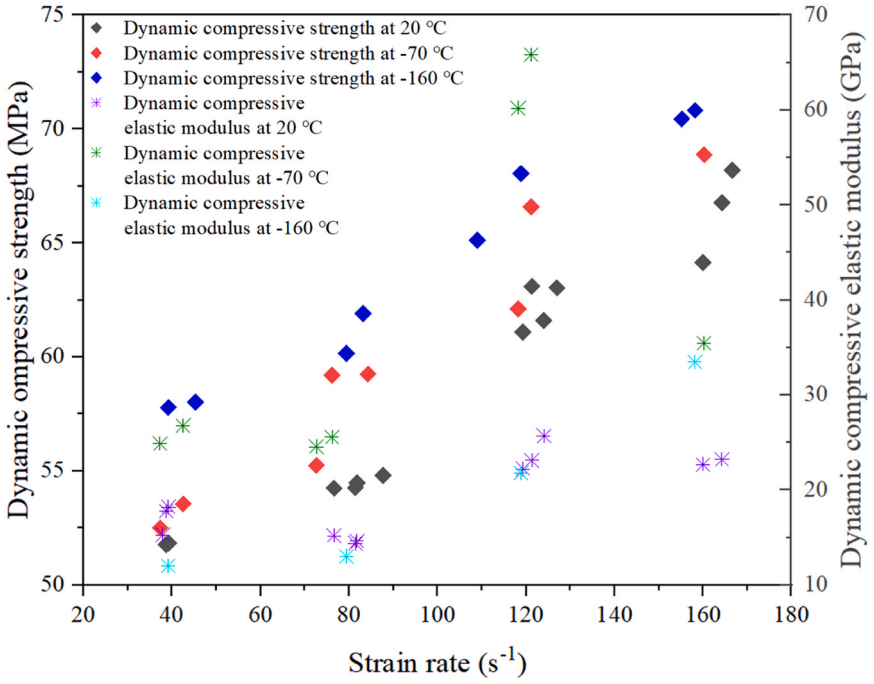


**Fig. 13.** Dynamic compressive strength and elastic modulus variation with temperature and strain rate.

between 30 % and 50 % of the peak strength from Fig. 12. Notably, at the same average strain rate, the elastic modulus at −70 °C was greater than that at room temperature and −160 °C. For instance, at an average strain rate of 80 $s^{-1}$, the elastic modulus at −70 °C was 1.76 times that at room temperature and 1.98 times than that at −160 °C. When the average strain rate was up to 160 $s^{-1}$, the elastic modulus at −70 °C was 1.56 times and 1.01 times greater than that at 20 and −160 °C, respectively. Similar findings have been observed in low-temperature static tests conducted by a few scholars [42,43]. Zhang *et al.*[42] explained this phenomenon by employing CT scanning to explore the microstructural alterations of concrete before and after exposure to low temperatures. It was noted that as temperatures declined within the −90 to −30 °C range, the elastic modulus enlarged due to the transition of a substantial volume of nanoscale pores' water to ice. However, when temperatures plummeted below −90 °C, these pores were entirely filled with ice, resulting in the formation of thermal cracks at the interfaces of ice and cement paste. Consequently, as temperatures decreased, the elastic modulus diminished.

### 3.3. Dynamic splitting tensile strength under combined loading

#### 3.3.1. Damage mode of specimens subjected to combined loading

Under various combinations of loading conditions with strain rates ranging from 20 to 80 $s^{-1}$ and temperatures of 20, −70, and −160 °C, significant changes in the dynamic splitting damage appearance of the specimens were observed, indicating a clear relationship between temperature and strain rate. Fig. 14 presents the damage patterns of NSM under dynamic splitting tension in different temperatures and strain rate scenarios. Specifically, at a strain rate of around 20 $s^{-1}$, secondary microcracks as well as small triangular fracture zones emerged at both ends of the specimen along the centre main crack, leading to its division into two parts. With further increase in strain rate, the triangular fracture area expanded gradually at both ends of the sample, accompanied by increased overall deformation. Notably, comparative analysis revealed that at equivalent strain rates, the damage severity at −70 °C surpassed that at room temperature.

When subjected to a temperature of −160 °C, the specimen exhibited increase brittleness as compared to its behaviour at room temperature. This heightened brittleness is clearly illustrated in Fig. 15, which depicted the dynamic fracturing process of NSM specimens under

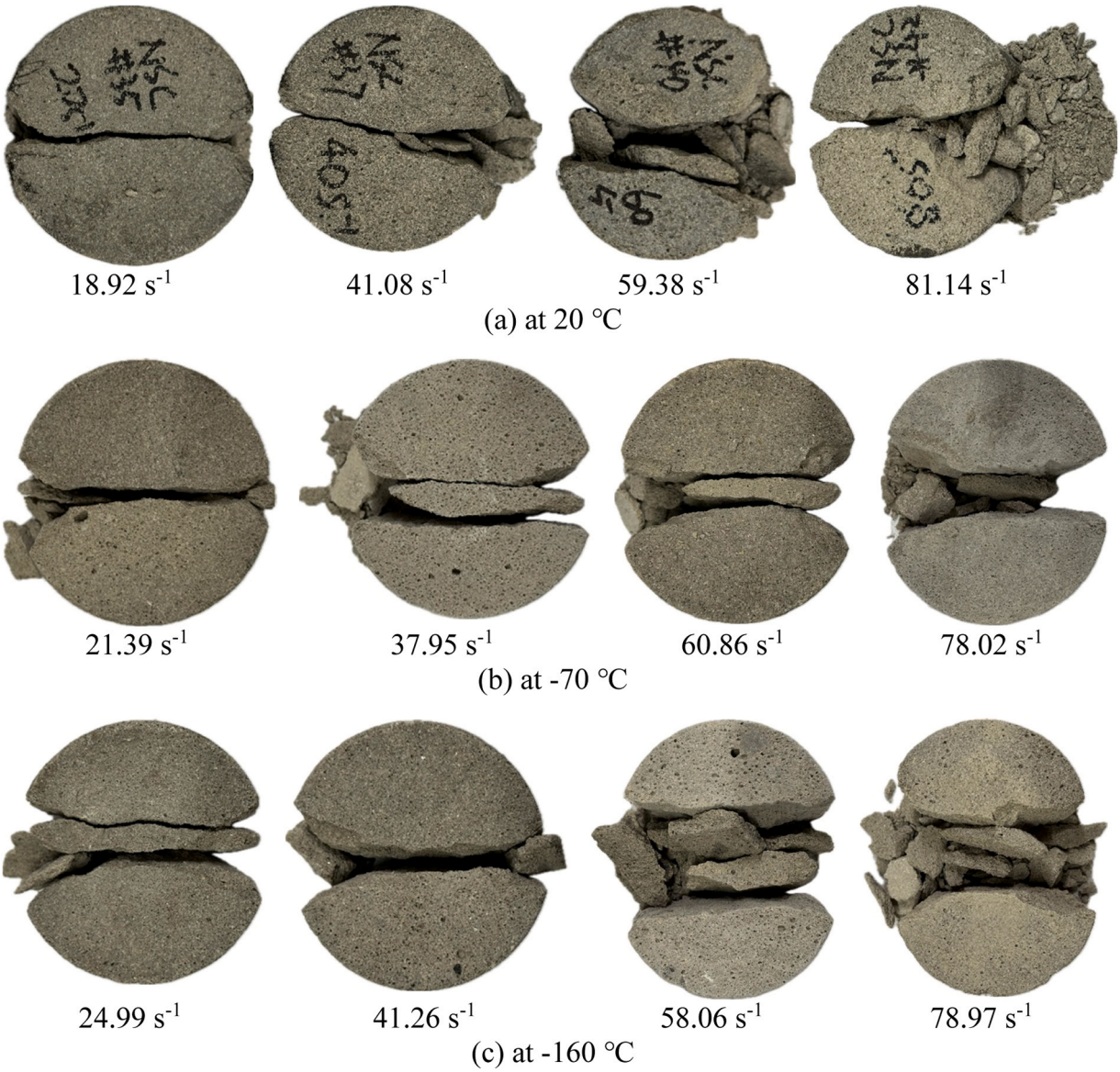


**Fig. 14.** Dynamic splitting tensile failure modes at different temperatures.

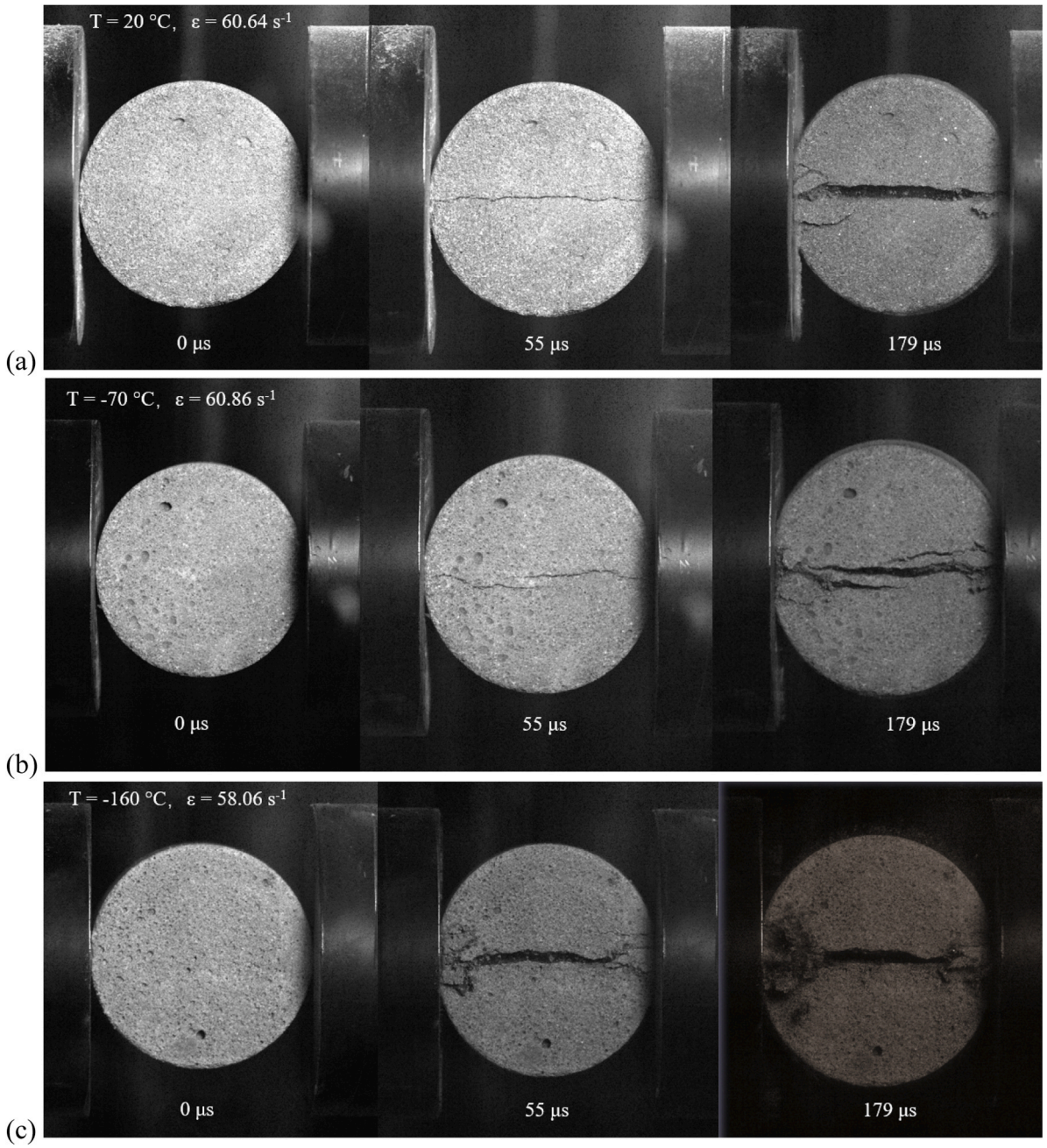


**Fig. 15.** Splitting tensile failure process of specimens under various temperatures. (a) at abmient temperature (b) at −70 °C (c) at −160 °C.

varying temperatures (20, −70, and −160 °C) with a strain rate of nearly 60 $s^{-1}$, captured using the ultra-high-speed video camera. At 55 μs, a primary crack formed along the loading and transmission rod directions. Notably, at −160 °C, the crack observed in the specimen was considerably larger than those observed at room temperature and −70 °C. Furthermore, secondary micro-cracks as well as small triangular fracture zones developed at the ends of the specimen along the primary crack, and the extent of damage intensified with time.

### *3.3.2. Influence of low and cryogenic temperature on dynamic splitting tensile strength*

The peak splitting tensile strength obtained from dynamic splitting tests at temperatures of 20, −70 and −160 °C along with strain rates of 20, 40, 60 and 80 $s^{-1}$ is depicted in Fig. 16. It was observed that at the same temperature, the splitting strength increased with strain rate. More specifically, at room temperature, the splitting strength increased by 17.03 %, 21.44 % and 31.40 % when the strain rate rose from approximately 20 $s^{-1}$ (18.92 $s^{-1}$) to 40 $s^{-1}$ (41.08 $s^{-1}$), 60 $s^{-1}$ (59.38 $s^{-1}$) and 80 $s^{-1}$ (81.14 $s^{-1}$), respectively. At −70 °C, the splitting strength increased by 25.36 %, 45.07 % and 51.58 %, with the strain rate increasing from approximately 20 $s^{-1}$ (21.39 $s^{-1}$) to 40 (37.95 $s^{-1}$), 60 (60.86 $s^{-1}$) and 80 $s^{-1}$ (78.02 $s^{-1}$), respectively. Likewise, at −160°C, the splitting strength escalated by 13.35 %, 27.57 % and 35.74 % as the strain rate increased from approximately 20 $s^{-1}$ (24.99 $s^{-1}$) to 40 (41.26 $s^{-1}$), 60 (58.06 $s^{-1}$) and 80 $s^{-1}$ (78.97 $s^{-1}$), respectively. Overall, these findings revealed that both temperature and strain rate visibly influenced the dynamic splitting strength of concrete, with lower temperatures and higher strain rates generally leading to higher splitting strength. Additionally, the rate and magnitude of strength increase varied with temperature, indicating complex temperature-dependent behaviour in dynamic splitting strength.

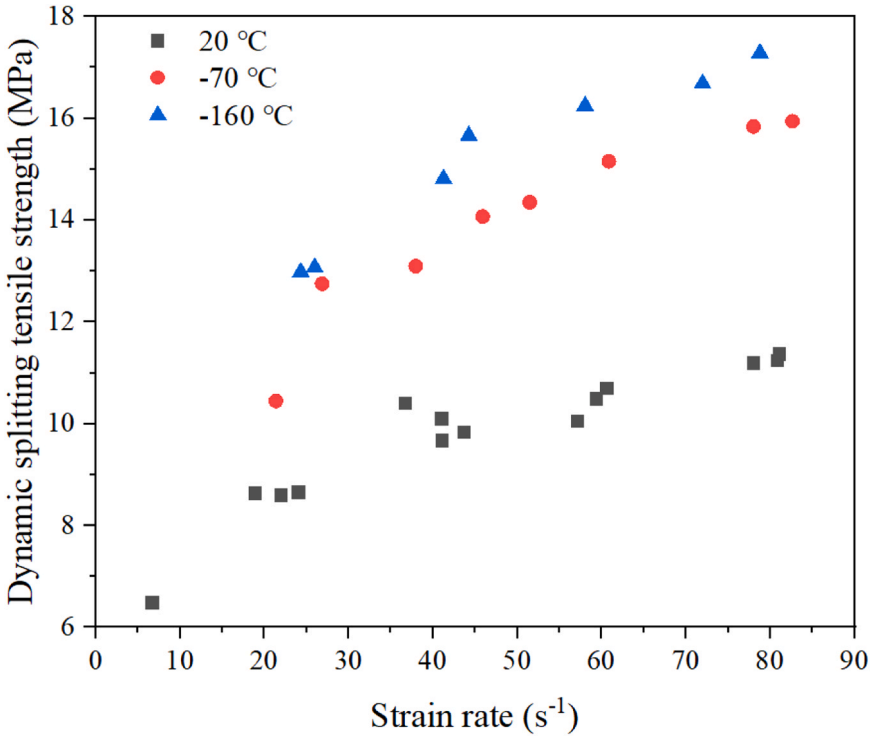


**Fig. 16.** Dynamic splitting tensile strength at different temperatures.

### 3.4. Dynamic behaviour NSM after cryogenic FT cycles

Understanding the dynamic behaviour of NSM subjected to cryogenic temperatures and FT cycles was essential for ensuring the safety and durability of structures cryogenic environments. In the current study, the dynamic compressive behaviour after 2, 4 and 8 FT cycles in the temperature range from −160–20 °C at high strain rate of 80, 130 and 180 $s^{-1}$ was investigated. Fig. 17 presents dynamic compressive strain-stress curves for mortar experienced different numbers of FT cycles. Fig. 17 (a) shows the strain-stress curves after 2 FT cycles, with strain rates of 82.76, 131.36 and 185.44 $s^{-1}$, whose peak strength was 51.53, 56.06 and 66.80 MPa, respectively. Fig. 17 (b) exhibits the strain-stress plots subsequent to 4 FT cycles, showcasing strain rates of 79.29, 127.77 and 175.17 $s^{-1}$, corresponding to peak strengths of 52.55, 53.79 and 62.72 MPa, respectively. Fig. 17 (c) illustrates the strain-stress curves following 8 FT cycles, featuring strain rates of 82.96, 128.56 and 180.29 $s^{-1}$, with peak strengths of 52.61, 54.19 and 58.46 MPa, respectively. A further reduction in peak stress can be observed with increased number of cryogenic FT cycles and a more gradual softening behaviour as compared to after 2 and 4 FT scenarios. For example, the dynamic compressive strength at strain rate around 180 $s^{-1}$ approximately reduced by 8.30 % and 14.57 % after 4 and 8 FT cycles, as compared to after 2 FT cycles.

### 3.5. Strain rate sensitivity

#### 3.5.1. Dynamic increase factor at low temperature

The influence of loading rate on material behaviour can be effectively quantified by the Dynamic Increase Factor (DIF) at various strain rates. The DIF expresses the ratio of the material's strength under dynamic loading (e.g., impact or blast) to its static strength. This concept examines the material response and identifies the critical loading rates experienced during high-velocity events.

The compressive strength dynamic increase factor (CDIFs) and splitting tensile strength dynamic increase factor (TDIFs) with temperature were examined, and an empirical formula was proposed to evaluate CDIFs and TDIFs of concrete at low temperatures in the range of 20 to −160 °C.

Extensive research has been done to explore the DIF of concrete material at ambient temperatures, such as CEB-FIP [44], Malvar and Crawford [45], Malvar and Ross [46] and Bischoff and Perry [47] etc. The DIF equation in compression for CEB-FIP [44] at 20 °C can be expressed as Eqs. (7) and (8). The equation demonstrated a bilinear relationship between DIF and the logarithm of strain rate, with a change in slope happening at a strain rate of 30 $s^{-1}$ with strain rate up to 300 $s^{-1}$.

$$DIF = \left(\frac{\dot{\varepsilon}}{\varepsilon_s}\right)^{1.026\alpha} \text{for} \dot{\varepsilon} \leq 30\text{s} - 1 \tag{7}$$

$$DIF = \gamma\left(\frac{\dot{\varepsilon}}{\varepsilon_s}\right)^{1/3} \text{for } \dot{\varepsilon} > 30\text{s} - 1 \tag{8}$$

where $\varepsilon_s$ is equal to $3\times\ 10^{-6}$ $s^{-1}$, $\alpha = \frac{1}{10+6f'_c/10}$ and $f'_c$is uniaxial compressive strength in MPa, $\gamma = 10^{(7.11\alpha-2.33)}$.

Grote *et al.* [27] conducted an experiment to analyse CDIF of mortar specimens whose diameter was 12.7 mm with a high strain rate from 250 to 1700 $s^{-1}$, as shown in Fig. 18. In addition, Zhang *et al.* [48] carried out CDIF of mortar with a specimen diameter of 37 mm. Chen *et al.* [28] also conducted a SHPB test to explore CDIF of mortar with a specimen diameter of 75 mm. It revealed that the strain rate sensitivity was lower for mortar as compared to NSC. Hao *et al.* [49] stated that increasing the volume fraction and size of aggregates in concrete led to higher heterogeneity, which resulted in a higher CDIF under high strain rates in contrast with concrete without or with smaller aggregates.

The data provided by Zhang et al. [48] and Chen et al. [28] were utilised for comparative analysis and validation. It could be observed that the experimental data at room temperature agreed well with the results from Zhang et al. [48] and Chen et al. [28], as shown in Fig. 18. Additionally, as the temperature decreased, the CDIFs also decreased. Specifically, at −70 °C and −160 °C, the CDIFs decreased by 13.45 % and 22.81 %, respectively, as compared to room temperature when considering a specific strain rate of 120 $s^{-1}$. This indicated that the

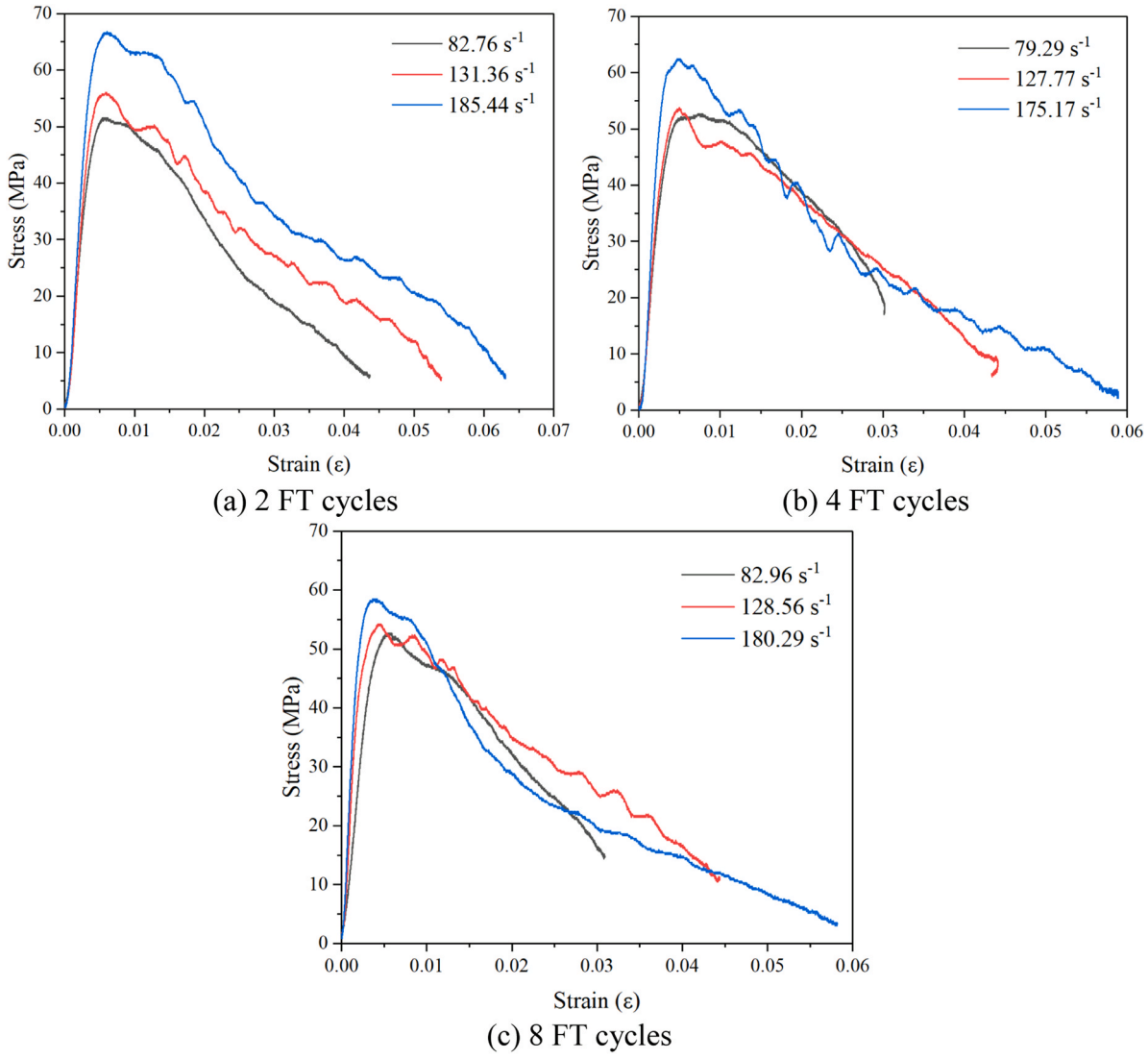


**Fig. 17.** Dynamic compressive strain-stress curve after various number of FT cycles.

sensitivity of concrete to loading rate decreased significantly at cryogenic temperatures as compared to room temperature. As the temperature declined, the compressive strength of concrete exhibited an increasing trend, whereas the CDIF displayed a decreasing pattern, lending support to the notion that the higher strength of the material was, the lower degree of rate sensitivity exhibited.

Moreover, this phenomenon could be explained by the formation of ice within the pore formation of the mortar. There was no ice in the pores of the mortar at ambient temperature. The behaviour of this material depended on its inherent characteristics, and the compressive strength was mainly influenced by the mortar composition and the strain rate applied during the testing process. While the temperature dropped to −70 °C, water in the mortar pores began to freeze, forming ice. The compressive and splitting strengths of ice were approximately 25 MPa and 3.1 MPa [50], which were similar to the static strength of mortar. The presence of ice raised the overall stiffness of the mortar. As the temperature of ice dropped from −15 to −125 °C or lower, the CDIF decreased [51]. However, at this time, ice has not yet fully dominated the influence on compressive strength. When the temperature dropped to −160 °C, the ice in the pores was much lower than the freezing point and became harder. At such low temperatures, ice signally affected the mechanical properties of mortar, resulting in lower CDIF as compared to −70 °C.

Following the fitting of the data points depicted in Fig. 18, Eqs. (9), (10) and (11) were formulated to plot the CDIF curves of NSM at room temperature, −70 and −160 °C, correspondingly. These derived curves were then compared with experimental data, illustrated in Fig. 18. It was worth noting that as the temperature decreased, the DIF decreased in compression. Furthermore, the transition strain rate was approximately 37.87 $s^{-1}$ at 20 °C, the change point occurred in 37.28 $s^{-1}$ at −70 °C, additionally, the transition strain rate exhibited in 55.21 $s^{-1}$ at −160 °C.

$$\text{CDIF at}20℃ = \begin{cases} 0.051\log\dot{\varepsilon} + 1.305 & \dot{\varepsilon} \le 37.87 \quad s^{-1} \\ 0.721\log\dot{\varepsilon} + 0.247 & \dot{\varepsilon} > 37.87 \quad s^{-1} \end{cases} \tag{9}$$

$$\text{CDIF at} -70℃ = \begin{cases} 0.021\log\dot{\varepsilon} + 1.128 & \dot{\varepsilon} \le 37.28 \quad s^{-1} \\ 0.644\log\dot{\varepsilon} + 0.148 & \dot{\varepsilon} > 37.28 \quad s^{-1} \end{cases} \tag{10}$$

$$\text{CDIF at} -160℃ = \begin{cases} 0.092\log\dot{\varepsilon} + 1.550 & \dot{\varepsilon} \le 55.21 \quad s^{-1} \\ 0.661\log\dot{\varepsilon} - 0.081 & \dot{\varepsilon} > 55.21 \quad s^{-1} \end{cases} \tag{11}$$

Fig. 19 displays the TDIFs at 20, −70, and −160 °C together with different strains. The experimental data of TDIFs at ambient temperature fitted well with those from Liu et al. [33] and Chen et al. [32], which demonstrated the accuracy and reliability of the tests. It was noteworthy that unlike CDIFs, TDIFs increased as the temperature decreased. TDIFs were enhanced at lower temperatures. Compared to room temperature,

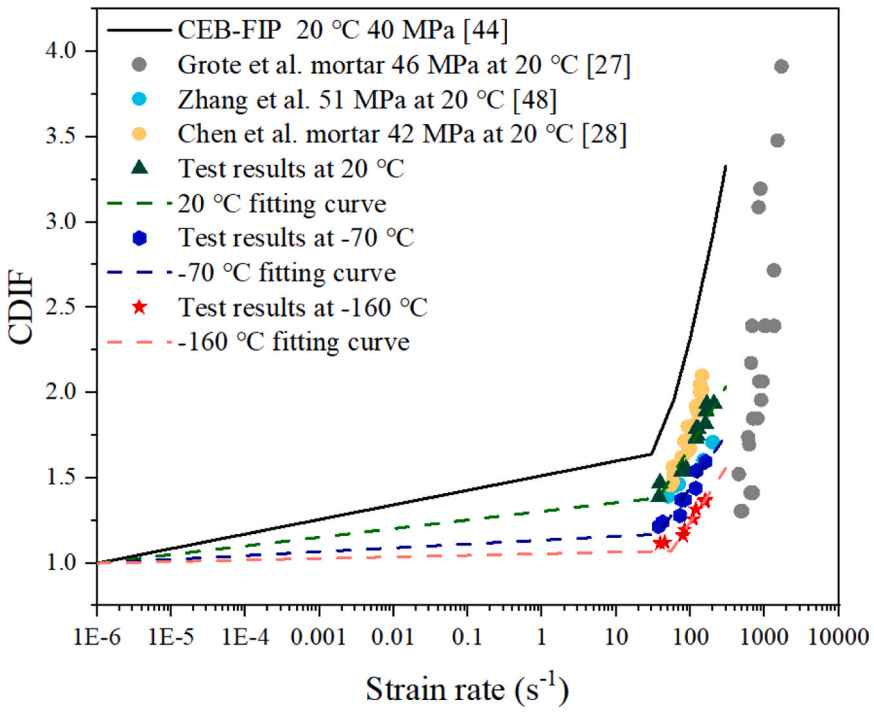


**Fig. 18.** Variation of CDIFs with strain rate at low and cryogenic temperature.

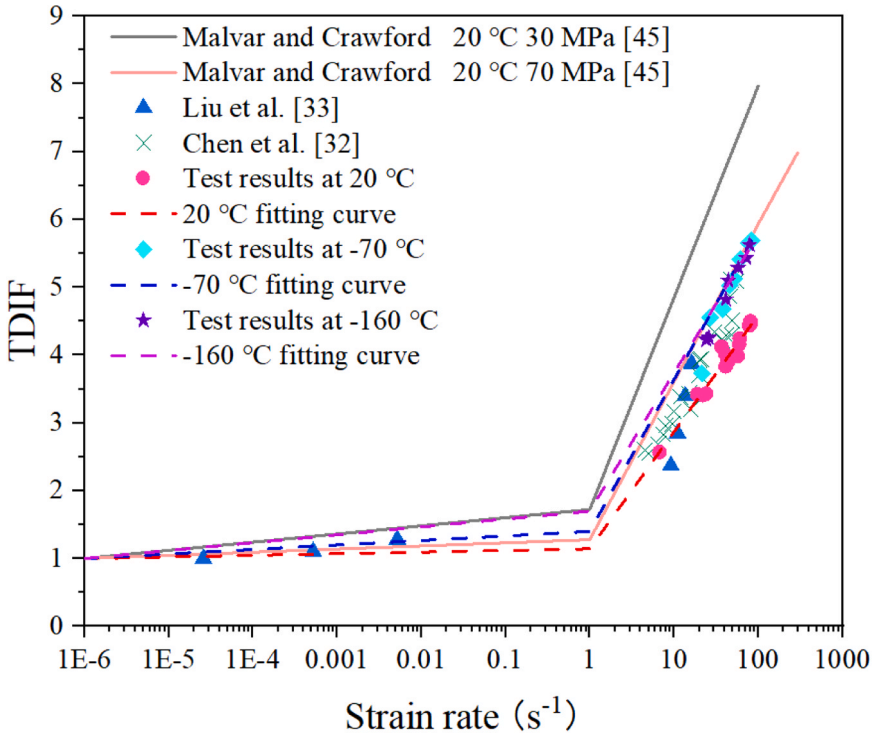


**Fig. 19.** Variation of TDIFs with strain rate at low temperature.

TDIFs at −70 and −160 °C increased by 30.36 % and 30.84 %, respectively, for a specific strain rate of 60 $s^{-1}$. In addition, the TDIFs were slightly greater at −160 °C than at −70 °C. This suggested that NSM exhibited a more sensitive strain rate response under dynamic splitting, highlighting the material's increased brittleness at lower temperatures.

After curve fitting the experimental data points at 20, −70 and −160 °C, the TDIF curves for the NSM at room temperature and −70 and −160 °C temperatures were developed separately in Eqs. (12), (13), (14), as shown in Figure19. The transition point for TDIF was set as 1 $s^{-1}$, which was the same as CEB-FIP [44] at 20 °C.

$$\text{TDIF at}20℃ = \begin{cases} 0.042\log\dot{\varepsilon} + 1.254 & \dot{\varepsilon} \le 1 \quad s^{-1} \\ 1.726\log\dot{\varepsilon} + 1.145 & \dot{\varepsilon} > 1 \quad s^{-1} \end{cases} \tag{12}$$

$$\text{TDIF at} -70℃ = \begin{cases} 0.083\log\dot{\varepsilon} + 1.500 & \dot{\varepsilon} \le 1 \quad s^{-1} \\ 2.548\log\dot{\varepsilon} + 0.804 & \dot{\varepsilon} > 1 \quad s^{-1} \end{cases} \tag{13}$$

$$\text{TDIF at} -160℃ = \begin{cases} 0.175\log\dot{\varepsilon} + 2.053 & \dot{\varepsilon} \le 1 \quad s^{-1} \\ 1.949\log\dot{\varepsilon} + 1.872 & \dot{\varepsilon} > 1 \quad s^{-1} \end{cases} \tag{14}$$

*3.5.2. Dynamic increase factor after cryogenic FT cycles*

Fig. 20 illustrates the DIFs with respect to strain rate (ranging from approximately 80 to 180 $s^{-1}$) after different numbers of cryogenic FT cycles. The regression equation for the fitting curve after 2 FT cycles was expressed as y = 1.207 log $\dot{\varepsilon}$ - 0.768. It was notable that the CDIF values following 2 FT cycles exhibited a slight elevation as compared to those at 20 °C. The fitting curve after 4 FT cycles followed the equation y = 0.774 log $\dot{\varepsilon}$ + 0.272. These CDIF values further rose as compared to those after 2 FT cycles, suggesting continued degradation in the material with increase FT cycles. The test results after 8 FT cycles were shown in the figure below, and the fitting curve was given by the equation y = 0.598 log $\dot{\varepsilon}$ + 0.839. The CDIF values after 8 FT cycles were the highest among the tested conditions, indicating the greatest strain rate sensitivity after 8 FT cycles, along with the most significant reduction of mortar owing to the cumulative effects of the FT cycles. The CDIFs after 4 and 8 cryogenic FT cycles increased approximately 11.63 % and 28.31 %, respectively, in contrast with that after 2 cryogenic FT cycles. Overall, the CDIF increased with the number of FT cycles, implying a reduction in the material's capability to resist dynamic loading after cryogenic FT cycles. During each FT cycle, water within the pore structure of concrete froze and expanded, resulting in the development of internal stresses. When the ice melted, it left behind microcracks and damage in the mortar. As the number of FT cycles increased, the extent of microcracking and internal damage accumulated, causing a higher CDIF.

## 4. SEM analysis after FT cycles

Scanning electron microscopy (SEM) was utilised to examine the microstructural changes and crack formation in fragments of samples after 2, 4 and 8 times of FT cycles (see Fig. 21). The microstructure appeared relatively intact with some pores and voids present when the sample without FT cycles. It was observed that, in comparison to the samples in the unfrozen state at room temperature, the samples subjected to 2 FT cycles exhibited an increase in the number of microscopic pores. After 4 FT cycles, the quantity and diameter of pores increased significantly, leading to severe deterioration of the mortar matrix (showing a fibrous texture), and the formation of microcracks was evident. Following 8 FT cycles, the number and diameter of pores continued to escalate, accompanied by an increase of microcracks. The loosened texture of the material after 8 FT cycles provided a key explanation for its heightened vulnerability to FT damage from a mechanistic standpoint. The observations aligned with the experimental results obtained by Xie and Wu [52] and Wei *et al.* [53]. To better understand the changing patterns of concrete pore characteristics, Zhou *et al.* [54] performed mercury intrusion porosimetry (MIP) and nuclear magnetic resonance (NMR) tests to analyse ordinary C60 concrete both before and after 20 FT cycles. The MIP results revealed a significant increase in pore volume in the concrete after 20 FT cycles, highlighting that internal pore water was a key factor influencing the mechanical behaviour. Similarly, the NMR results indicated a marked rise in the number of large capillary pores and considerable structural deterioration in the concrete. This consistency in observed trends and damage mechanisms across different studies reinforces the validity of the findings from SEM.

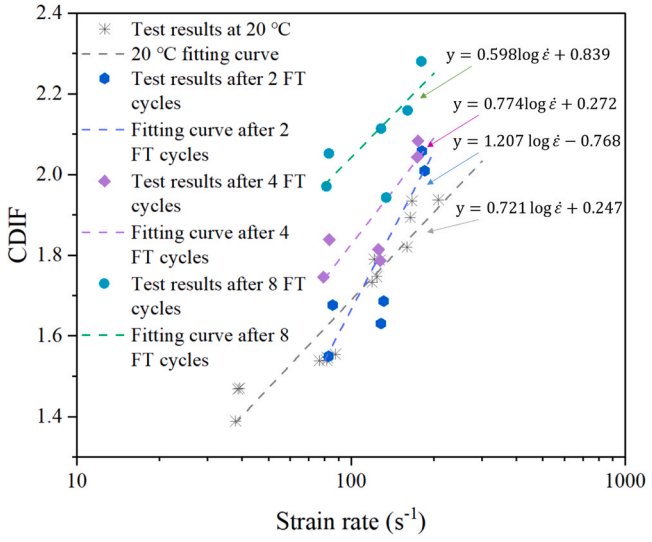


**Fig. 20.** Variation in CDIFs with strain rate after different numbers of FT cycles.

In conclusion, it emphasised that FT cycles had a significant and progressive effect on the microstructure of the samples, leading to increased porosity, deterioration of the mortar matrix, and the formation and propagation of microcracks. These microstructural changes can have detrimental effects on the mechanical properties and durability of the material, potentially compromising its performance and service life in environments subjected to freezing and thawing conditions.

## 5. Conclusions and recommendations for future research work

This study investigated the dynamic mechanical properties of NSM under extreme temperature conditions (20, −70 and −160 °C) and after cryogenic FT cycles in temperature range from −160–20 °C using SHPB tests. The following particular conclusions can be drawn:

- At −70 and −160 °C, the severity of damage decreased as compared to room temperature, indicating improved impact resistance. Additionally, the stiffness of the material increased at lower temperatures, leading to reduced deformation and damage.
- Dynamic compressive strength increased with strain rate at all temperatures, with higher strain rates resulting in considerable enhancements in strength. The modulus of elasticity also increased at lower temperatures, indicating a more rigid response of NSM at extremely cold temperatures.
- The splitting strength increased with strain rate and decreasing temperature. Lower temperatures (-70 °C and −160 °C) led to higher splitting strength than room temperature, indicating enhanced resistance to dynamic tensile loading at extremely cold temperatures.
- While dynamic strengths generally increased with higher strain rates, the sensitivity to strain rate decreased significantly at cryogenic temperatures for compression, as evidenced by decreasing CDIFs. The results showed that the CDIFs at −70 and −160 °C decreased by about 12.63 % and 24.7 % as compared to at 20 °C when the strain rate was 160 $s^{-1}$. Conversely, dynamic splitting exhibited increased rate sensitivity at lower temperatures, reflected in increasing TDIFs. The experimental results indicated that the TDIFs at −70 and −160 °C had a rise of 16.71 % and 29.72 % as compared to 20 °C when the strain rate was approximately 40 $s^{-1}$.
- The increase number of cryogenic FT cycles resulted in a notable increase in the strain rate sensitivity of concrete and decrease its ability to withstand dynamic loading. At the strain rate of 180 $s^{-1}$, the DIFs after 8 FT cycles were approximately 13.43 % and 9.62 % greater than after 2 and 4 times FT cycles, respectively.

To further understand the microstructural changes under and after cryogenic loading, NMR or MIP will be employed in future studies. These advanced techniques can provide quantitative data on pore number and pore structure, offering deeper insights into the mechanisms of FT damage in concrete.

Additionally, further analysis is needed to investigate the TDIFs

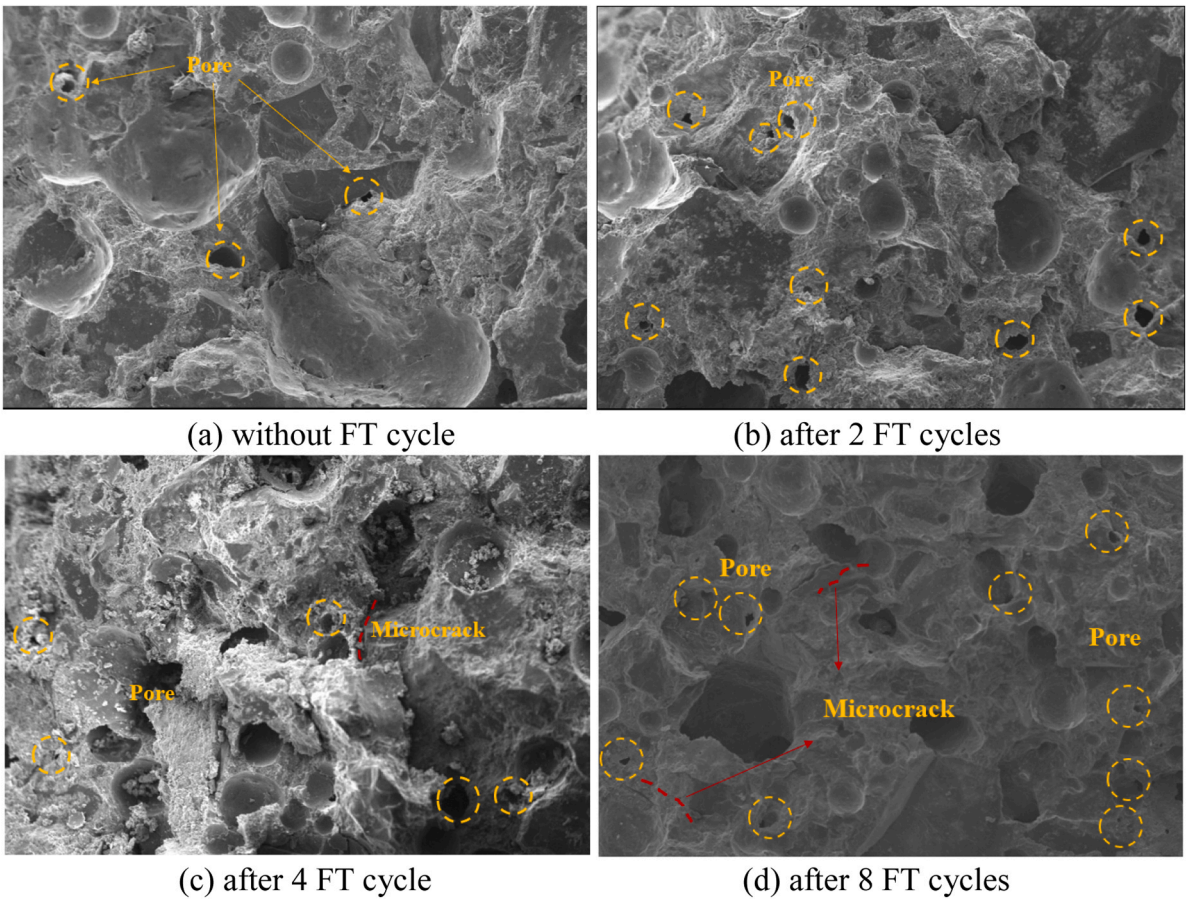


**Fig. 21.** Microscopic image of samples after various number of FT cycles.

under low temperature. Understanding why TDIFs exhibit improvement under these conditions could reveal critical information about the behaviour and resilience of material, contributing to the optimisation of concrete performance in cryogenic environments.

## CRediT authorship contribution statement

**Kaiyi Chi:** Writing – original draft, Validation, Methodology, Investigation, Formal analysis, Data curation. **Jun Li:** Writing – review & editing, Supervision, Project administration, Methodology, Investigation, Conceptualization. **Ruizhe Shao:** Writing – review & editing, Methodology, Investigation. **Longyang Chen:** Software, Resources. **Shenchun Xu:** Methodology, Investigation. **Chengqing Wu:** Writing – review & editing, Supervision, Resources, Project administration, Methodology, Investigation, Conceptualization.

## Declaration of Competing Interest

The authors declare that they have no known competing financial interests or personal relationships that could have appeared to influence the work reported in this paper.

## Data availability

Data will be made available on request.

## Acknowledgement

The study presented in this study is supported by the Australian Research Council (ARC) Discovery Projects (DP) Grant DP210101100.

## Appendix A. Test results of compression SHPB test at 20, −70 and −160 °C

| Temperature ($T$) | Strain rate ($s^{-1}$) | Dynamic compressive strength ($f'_c$) | CDIF |
|---|---|---|---|
| 20 °C | 24.61 | 41.68 | 1.18 |
| | 37.87 | 48.97 | 1.39 |
| | 39.18 | 51.85 | 1.47 |
| | 38.63 | 51.77 | 1.47 |
| | 76.60 | 54.25 | 1.54 |
| | 81.45 | 54.27 | 1.54 |
| | 81.81 | 54.5 | 1.55 |
| | 87.65 | 54.82 | 1.55 |
| | 119.30 | 61.10 | 1.73 |

(*continued on next page*)

(*continued*)

| Temperature ($T$) | Strain rate ($s^{-1}$) | Dynamic compressive strength ($f'_c$) | CDIF |
|---|---|---|---|
| | 121.30 | 63.10 | 1.79 |
| | 124.01 | 61.60 | 1.75 |
| | 127.00 | 63.03 | 1.79 |
| | 159.97 | 64.15 | 1.82 |
| | 164.28 | 66.77 | 1.89 |
| | 166.63 | 68.19 | 1.93 |
| | 207.85 | 68.30 | 1.94 |
| -70 °C | 37.28 | 52.51 | 1.22 |
| | 42.51 | 53.56 | 1.24 |
| | 72.60 | 55.24 | 1.28 |
| | 76.13 | 59.20 | 1.37 |
| | 84.25 | 59.25 | 1.37 |
| | 118.21 | 62.11 | 1.44 |
| | 121.11 | 66.59 | 1.54 |
| | 160.22 | 68.88 | 1.59 |
| -160 °C | 39.10 | 57.78 | 1.12 |
| | 45.26 | 58.03 | 1.12 |
| | 79.38 | 60.15 | 1.16 |
| | 83.13 | 61.91 | 1.20 |
| | 108.99 | 65.14 | 1.26 |
| | 118.88 | 68.05 | 1.31 |
| | 155.16 | 70.44 | 1.36 |
| | 158.19 | 70.82 | 1.37 |

## Appendix B. Test results of splitting tensile SHPB test at 20, −70 and −160 °C

| Temperature ($T$) | Strain rate ($s^{-1}$) | Dynamic splitting tensile strength ($f'_T$) | TDIF |
|---|---|---|---|
| 20 °C | 6.73 | 6.48 | 2.57 |
| | 18.92 | 8.63 | 3.42 |
| | 22.03 | 8.59 | 3.41 |
| | 24.09 | 8.65 | 3.43 |
| | 36.77 | 10.40 | 4.13 |
| | 41.08 | 10.10 | 4.01 |
| | 41.15 | 9.66 | 3.83 |
| | 43.76 | 9.84 | 3.90 |
| | 57.2 | 10.05 | 3.99 |
| | 59.38 | 10.48 | 4.16 |
| | 60.64 | 10.69 | 4.24 |
| | 78.05 | 11.18 | 4.44 |
| | 80.90 | 11.24 | 4.46 |
| | 81.14 | 11.36 | 4.50 |
| -70 °C | 21.39 | 10.45 | 3.73 |
| | 26.86 | 12.75 | 4.55 |
| | 37.95 | 13.10 | 4.68 |
| | 45.91 | 14.07 | 5.03 |
| | 51.49 | 14.35 | 5.13 |
| | 60.86 | 15.16 | 5.41 |
| | 78.02 | 15.84 | 5.66 |
| | 82.64 | 15.94 | 5.69 |
| -160 °C | 24.32 | 12.98 | 4.23 |
| | 25.99 | 13.07 | 4.26 |
| | 41.26 | 14.81 | 4.82 |
| | 44.26 | 15.66 | 5.10 |
| | 58.06 | 16.24 | 5.29 |
| | 71.97 | 16.68 | 5.43 |
| | 78.79 | 17.28 | 5.63 |

## Appendix C. Test results of compressive SHPB test after cryogenic FT cycles

| Temperature range | NO. FT | Strain rate | Dynamic compressive strength ($f'_c$) | DIF |
|---|---|---|---|---|
| -160–20 °C | 2 | 82.76 | 51.53 | 1.55 |
| | | 85.62 | 55.74 | 1.68 |
| | | 128.47 | 54.22 | 1.63 |
| | | 131.36 | 56.06 | 1.69 |
| | | 181.25 | 68.43 | 2.06 |

(*continued on next page*)

(*continued*)

| Temperature range | NO. FT | Strain rate | Dynamic compressive strength ($f'_c$) | DIF |
|---|---|---|---|---|
| | | 185.44 | 66.80 | 2.01 |
| | 4 | 83.21 | 55.35 | 1.84 |
| | | 79.29 | 52.55 | 1.75 |
| | | 127.77 | 53.79 | 1.79 |
| | | 125.87 | 54.62 | 1.81 |
| | | 175.17 | 62.72 | 2.08 |
| | | 174.22 | 61.51 | 2.04 |
| | 8 | 81.22 | 50.52 | 1.97 |
| | | 82.96 | 52.61 | 2.05 |
| | | 128.56 | 54.19 | 2.11 |
| | | 134.16 | 49.81 | 1.94 |
| | | 160.65 | 55.35 | 2.16 |
| | | 180.29 | 58.46 | 2.28 |

## References


[1] N. Krstulovic-Opara, Liquefied natural gas storage: Material behavior of concrete at cryogenic temperatures, Acids Mater. J. 104 (3) (2007) 297.
[2] R.B. Kogbara, S.R. Iyengar, Z.C. Grasley, E.A. Masad, D.G. Zollinger, A review of concrete properties at cryogenic temperatures: towards direct LNG containment, Constr. Build. Mater. 47 (2013) 760–770.
[3] Y. Zhu, H. Yang, S. Zhang, Dynamic mechanical behavior and constitutive models of S890 high-strength steel at intermediate and high strain rates, J. Mater. Eng. Perform. 29 (2020) 6727–6739.
[4] T.J. MacLean, A. Lloyd, High strain rate and low temperature effects on the compressive behaviour of concrete, Int. J. Prot. Struct. 12 (1) (2021) 73–94.
[5] Y. Goto, T. Miura, Deterioration of concrete subjected to repetitions of very low temperatures, Trans. Jpn. Concr. Inst. (1979) 183–190.
[6] Y. Goto, T. Miura, Mechanical properties of concrete at very low temperatures, Proc. 21st Jpn. Congr. Mater. Res. (1978).
[7] Monfore, G. and A. Lentz, Physical properties of concrete at very low temperatures. 1962: Portland Cement Association.
[8] K. MITSUI, T. YONEZAWA, I. TAKAYUKI, Mechanical properties of high strength concrete under cryogenic atmosphere, Proc. Jpn. Concr. Inst. (Janpanese) 19 (1) (1997) 175–180.
[9] L. Dahmani, A. Khenane, S. Kaci, Behavior of the reinforced concrete at cryogenic temperatures, Cryogenics 47 (9-10) (2007) 517–525.
[10] F. Rostásy, U. Pusch, Strength and deformation of lightweight concrete of variable moisture content at very low temperatures, Int. J. Cem. Compos. Lightweight Concr. 9 (1) (1987) 3–17.
[11] J. Xie, J. Yan, Experimental studies and analysis on compressive strength of normal-weight concrete at low temperatures. Struct. Concr. 19 (4) (2018) 1235–1244.
[12] G. Lee, T. Shih, K.-C. Chang, Mechanical properties of concrete at low temperature, J. Cold Reg. Eng. 2 (1) (1988) 13–24.
[13] H. Lin, Y. Han, S. Liang, F. Gong, S. Han, C. Shi, P. Feng, Effects of low temperatures and cryogenic freeze-thaw cycles on concrete mechanical properties: a literature review, Constr. Build. Mater. 345 (2022) 128287.
[14] Y. Huo, H. Sun, D. Lu, Z. Chen, Y. Yang, Mechanical properties of concrete at low and ultra-low temperatures-a review, J. Infrastruct. Preserv. Resil. 3 (1) (2022) 1–15.
[15] Wiedemann, G., Zum Einfuss Tiefer Temperaturen auf Festigkeitund Verformung von Beton in Institute for Building Materials, Solid Construction, and Fire Protection. 1982, Technical University of Braunschweig.
[16] F. Gong, Y. Wang, T. Ueda, D. Zhang, Modeling and mesoscale simulation of ice-strengthened mechanical properties of concrete at low temperatures, J. Eng. Mech. 143 (6) (2017) 04017022.
[17] F. Gong, T. Ueda, D. Zhang, Two-dimensional rigid body spring method based micro-mesoscale study of mechanical strengthening/damaging effects to concrete by frost action, Struct. Concr. 19 (4) (2018) 1131–1145.
[18] J. Zhengwu, D. Zilong, Z. Xinping, L. Wenting, Increased strength and related mechanisms for mortars at cryogenic temperatures, Cryogenics 94 (2018) 5–13.
[19] V. Van de Veen, Properties of concrete at very low temperatures: A survey of the literature. Report Stevin laboratory, Concr. Struct. (1987) 25–87-2.
[20] X. Shi, J. Li, W. Wang, L. Qian, C. Ma, Experimental study on stress-strain relationships of concrete undergoi °C, Concrete (Chin.) 12 (2017) 1–5.
[21] X. Shi, W. Wang, J. Tian, Experimental study on the compressive strength of concrete of different strength grades experiencing ultralow temperature freeze-thaw cycle action, Eng. Mech. (Chin.) 37 (2) (2020) 211–220.
[22] X. Shi, Y. LI, L. QIAN, J. LI, W. WANG, Experimental Study on elastic modulus of concrete undergoing freeze-thaw cycle action with different ultralow temperature ranges, Eng. Mech. (Chin.) 36 (8) (2019) 106–113.
[23] D. Huang, Y. Feng, Q. Xia, J. Tian, X. Li, Research on mechanical properties and durability of early frozen concrete: a review, Constr. Build. Mater. 425 (2024) 135988.
[24] K. Chi, J. Li, C. Wu, Behaviour of reinforced concrete panels under impact loading after cryogenic freeze-thaw cycles, Constr. Build. Mater. 414 (2024) 135058.
[25] Z. Jiang, B. He, X. Zhu, Q. Ren, Y. Zhang, State-of-the-art review on properties evolution and deterioration mechanism of concrete at cryogenic temperature, Constr. Build. Mater. 257 (2020) 119456.
[26] F. Rostasy, U. Schneider, G. Wiedemann, Behaviour of mortar and concrete at extremely low temperatures, Cem. Concr. Res. 9 (3) (1979) 365–376.
[27] D. Grote, S. Park, M. Zhou, Dynamic behavior of concrete at high strain rates and pressures: I. experimental characterization, Int. J. Impact Eng. 25 (9) (2001) 869–886.
[28] X. Chen, S. Wu, J. Zhou, Experimental and modeling study of dynamic mechanical properties of cement paste, mortar and concrete, Constr. Build. Mater. 47 (2013) 419–430.
[29] Y. Guo, G. Gao, L. Jing, V. Shim, Dynamic properties of mortar in high-strength concrete, Int. J. Impact Eng. 165 (2022) 104216.
[30] Y.-j Xie, Q. Fu, K.-r Zheng, Q. Yuan, H. Song, Dynamic mechanical properties of cement and asphalt mortar based on SHPB test, Constr. Build. Mater. 70 (2014) 217–225.
[31] X. Zhang, Y.-w Chiu, H. Hao, J. Cui, Free water effect on the dynamic compressive properties of mortar, Cem. Concr. Compos. 118 (2021) 103933.
[32] X. Chen, Y. Shao, L. Xu, C. Chen, Experimental study on tensile behavior of cement paste, mortar and concrete under high strain rates, J. Wuhan. Univ. Technol. -Mater. Sci. Ed. 30 (6) (2015) 1268–1273.
[33] P. Liu, X. Zhou, Q. Qian, F. Berto, L. Zhou, Dynamic splitting tensile properties of concrete and cement mortar, Fatigue Fract. Eng. Mater. Struct. 43 (4) (2020) 757–770.
[34] L. Fenu, D. Forni, E. Cadoni, Dynamic behaviour of cement mortars reinforced with glass and basalt fibres, Compos. Part B: Eng. 92 (2016) 142–150.
[35] L. Jin, K. Liu, R. Zhang, W. Yu, X. Du, X. Deng, Combined effects of cryogenic temperature and strain rates on compressive behavior of concrete, Int. J. Damage Mech. 31 (9) (2022) 1396–1419.
[36] Y. Qiao, H. Wang, L. Cai, W. Zhang, B. Yang, Influence of low temperature on dynamic behavior of concrete, Constr. Build. Mater. 115 (2016) 214–220.
[37] X. Shi, L. Qian, C. Ma, J. LI, W. Wang, Experimental study on the temperature field of concrete during cooling from room temperature to-196°C and then returning to room temperature. Eng. Mech. (Chin.) 35 (5) (2018) 162–169.
[38] P. Follansbee, C. Frantz, Wave propagation in the split Hopkinson pressure bar, J. Eng. Mater. Technol. 105 (1983).
[39] H. Kolsky, An investigation of the mechanical properties of materials at very high rates of loading, Proc. Phys. Soc. Sect. B 62 (11) (1949) 676.
[40] U. Lindholm, Some experiments with the split hopkinson pressure bar*, J. Mech. Phys. Solids 12 (5) (1964) 317–335.
[41] J. Yan, J. Xie, Behaviours of reinforced concrete beams under low temperatures, Constr. Build. Mater. 141 (2017) 410–425.
[42] D. Zhang, J. Niu, P. Chen, P. Ranjith, W. Nie, Mechanical properties of concrete under different water content and low temperature conditions, Mater. Struct. 56 (4) (2023) 71.
[43] J. Marechal, Variations in the modulus of elasticity and Poisson's ratio with temperature, Spec. Publ. 34 (1972) 495–504.
[44] CEB-FIP, Model Code *1990* for Concrete Structures, Comit e Euro-International du B eton and F ed eration Internationale de la Pr econtrainte. 1993, Thomas Telford, London.
[45] L.J. Malvar, J.E. Crawford, Dynamic increase factors for concrete. DTIC document 1 (1.4) (1998) 1.6.
[46] L.J. Malvar, Review of static and dynamic properties of steel reinforcing bars, Mater. J. 95 (5) (1998) 609–616.
[47] P. Bischoff, S. Perry, Compressive behaviour of concrete at high strain rates, Mater. Struct. 24 (1991) 425–450.
[48] M. Zhang, H. Wu, Q. Li, F. Huang, Further investigation on the dynamic compressive strength enhancement of concrete-like materials based on split Hopkinson pressure bar tests. Part I: experiments, Int. J. Impact Eng. 36 (12) (2009) 1327–1334.

[49] Y. Hao, H. Hao, G. Jiang, Y. Zhou, Experimental confirmation of some factors influencing dynamic concrete compressive strengths in high-speed impact tests, Cem. Concr. Res. 52 (2013) 63–70.
[50] J. Petrovic, Review mechanical properties of ice and snow, J. Mater. Sci. 38 (2003) 1–6.
[51] X. Wu, V. Prakash, Dynamic compressive behavior of ice at cryogenic temperatures, Cold Reg. Sci. Technol. 118 (2015) 1–13.
[52] J. Xie, H. Wu, Experimental research on concrete strength under freeze–thaw recycle action with ultra-low temperature, J. Civ. Archit. Environ. Eng. 34 (2012) 165–168.
[53] Q. Wei, J. Xie, H. Wu, Experimental analysis on properties of concrete after freeze-thaw cycles under extra-low temperatures, Eng. Mech. (Chin.) 30 (Special issue) (2013) 125–131.
[54] D. Zhou, J. Liu, P. Duan, L. Cheng, B. Lou, Damage evolution law an mechanism of concrete under cryogenic freeze-thaw cycles, J. Build. Mater. (2021) 1–13.